The Asian Monsoon, the Tropospheric Biennial Oscillation, and the Indian Ocean Zonal Mode in the NCAR CSM*

JOHANNES LOSCHNIGG

International Pacific Research Center, School of Ocean and Earth Science and Technology, University of Hawaii at Manoa, Honolulu, Hawaii

GERALD A. MEEHL

National Center for Atmospheric Research,+ Boulder, Colorado

PETER J. WEBSTER

Program in Atmospheric and Oceanic Sciences, University of Colorado, Boulder, Colorado

JULIE M. ARBLASTER

National Center for Atmospheric Research, Boulder, Colorado

GILBERT P. COMPO

NOAA–CIRES Climate Diagnostics Center, University of Colorado, Boulder, Colorado

(Manuscript received 4 January 2002, in final form 18 November 2002)

ABSTRACT

The interaction of the Indian Ocean dynamics and the tropospheric biennial oscillation (TBO) is analyzed in the 300-yr control run of the National Center for Atmospheric Research (NCAR) Climate System Model (CSM). Sea surface temperature (SST) anomalies and equatorial ocean dynamics in the Indian Ocean are associated with the TBO and interannual variability of Asian–Australian monsoons in observations. The air–sea interactions involved in these processes in the coupled ocean–atmosphere model are analyzed, so as to diagnose the causes of the SST anomalies and their role in the development of a biennial cycle in the Indian–Pacific Ocean region.

By using singular value decomposition (SVD) analysis, it is found that the model reproduces the dominant mechanisms that are involved in the development of the TBO's influence on the south Asian monsoon: large-scale forcing from the tropical Pacific and regional forcing associated with both the meridional temperature gradient between the Asian continent and the Indian Ocean, as well as Indian Ocean SST anomalies. Using cumulative anomaly pattern correlation, the strength of each of these processes in affecting the interannual variability of both Asian and Australian monsoon rainfall is assessed.

In analyzing the role of the Indian Ocean dynamics in the TBO, it is found that the Indian Ocean zonal mode (IOZM) is an inherent feature of the Asian summer monsoon and the TBO. The IOZM is thus a part of the biennial nature of the Indian–Pacific Ocean region. The coupled ocean–atmosphere dynamics and cross-equatorial heat transport contribute to the interannual variability and biennial nature of the ENSO–monsoon system, by affecting the heat content of the Indian Ocean and resulting SST anomalies over multiple seasons, which is a key factor in the TBO.

1. Introduction

The interannual variability of the Asian–Australian monsoon system has been a focus of substantial research in recent decades because of the influence of the monsoon on the global climate and its interaction with the El Niño–Southern Oscillation (ENSO) phenomenon. Recently, the tropospheric biennial oscillation (TBO) has been shown to contribute to climate variations in the Indian and Pacific Ocean regions on interannual timescales. The relationship of ocean dynamics in the tropical Indian Ocean region to these large-scale climate variations in the ENSO–monsoon system associated with the TBO in the National Center for Atmospheric Research (NCAR) coupled Climate System Model (CSM) will be the primary focus of this paper.

The TBO has been defined as the tendency for the

* School of Ocean and Earth Sciences Contribution Number 6116 and International Pacific Research Center Contribution Number 196.
+ The National Center for Atmospheric Research is sponsored by the National Science Foundation.

Corresponding author address: Johannes Loschnigg, IPRC/SOEST, University of Hawaii at Manoa, 2525 Correa Road, Honolulu, HI 96822.
E-mail: johannes@soest.hawaii.edu

Asian monsoon to alternate between ''strong'' and ''weak'' years. Thus the TBO encompasses ENSO years that also have a similar biennial relationship to the Asian–Australian monsoon. The transitions between the years in this cycle are characterized by large-scale coupled land–ocean–atmosphere interactions in the Indian and Pacific Ocean regions (Meehl 1997). Both observational (Yasunari 1990, 1991; Ropelewski et al. 1992; Yasunari and Seki 1992; Yang et al. 1996; Tomita and Yasunari 1996; Meehl 1987, 1997; Webster et al. 1998) and modeling studies (Ogasawara et al. 1999; Kitoh et al. 1999; Chang and Li 2000; Li et al. 2001) have attempted to describe the basic processes involved in the biennial nature of the tropical climate in this region, and various theories have been given to assess the causes of the TBO (Meehl 1987, 1993, 1994; Goswami 1995; Webster et al. 1998; Kawamura et al. 2001; Clarke et al. 1998; Kim and Lau 2001). Recent studies have attempted to quantify the strength of the contributions of various local and remote forcings on the TBO (Meehl and Arblaster 2002b), as well as isolating the coupled features involved in the transition of the TBO from a year of one sign anomalies to the other (Meehl and Arblaster 2002a).

In this paper we will focus on how the ocean dynamics in the tropical Indian Ocean contribute to the development of sea surface temperature (SST) anomalies on interannual timescales, and thus contribute to the biennial variability in the Indian–Pacific Ocean climate. Because of the heat storage and consequent memory of the ocean, various oceanic dynamical processes associated with the TBO help develop and maintain SST anomalies over multiple seasons, a key aspect of the biennial cycle. Loschnigg and Webster (2000) and Webster et al. (2003, manuscript submitted to *Quart. J. Roy. Meteor. Soc.*, hereafter W03) have shown that the variability of the Indian Ocean is in the form of distinct and slowly varying dynamic modes and not just localized mixing as originally argued by Meehl (1987). The presence of Indian Ocean SST anomalies has been central to many of the theories of the TBO (e.g., Meehl 1997; Chang and Li 2000), and the development of an equatorial SST gradient in the boreal fall season—along with the existence of equatorial wave dynamics that contribute to thermocline depth anomalies and enhance SST anomalies—has been associated with the strong and weak monsoon cycle and ENSO variability in descriptions of the TBO cycle [Meehl et al. (2003), hereafter MAL; W03]. The existence of an Indian Ocean zonal mode (IOZM) of equatorial SST anomalies has been given much attention after the particularly strong event in 1997/98, concurrent with the strong El Niño event of that year (Webster et al. 1999; Saji et al. 1999). It has been suggested that this mode of SST anomalies, which has also been termed the ''dipole mode,'' is an independent mode not associated with ENSO (Iizuka et al. 2000). But recent studies suggest that the mode of SST variability is more of a southern Indian Ocean phenomena (Behera et al. 2000), that the mode is not purely independent of ENSO (Baquero-Bernal et al. 2002; Nicholls 2001) or that the IOZM is an integral part of the TBO (Meehl and Arblaster 2002b). Even in the studies that question the existence of an independent mode, the results suggest an equatorial SST anomaly gradient in the Indian Ocean during the boreal fall season, which will be discussed later as being connected to the ENSO–monsoon system. In observational studies (Meehl and Arblaster 2002b), ocean dynamics in the Indian Ocean are associated with TBO springtime transition as well as SST anomalies occurring in the equatorial regions. Thus ocean dynamics are likely associated with extremes of Indian Ocean dipole events that are a natural part of the TBO evolution. In this study, we will be analyzing the influence of the ocean dynamics in a coupled model in this region, and its relation to the Indian Ocean SST dipole, the Asian monsoon, ENSO, and the TBO.

The large-scale meridional oceanic heat transport in the Indian Ocean has been studied on both seasonal (Hsiung et al. 1989; Hastenrath and Greischar 1993; Wacongne and Pacanowski 1996; Loschnigg and Webster 2000) and interannual (Garternicht and Schott 1997; Lee and Marotzke 1997; Loschnigg and Webster 2000) timescales. It has been shown that the heat transport modulates the northern Indian Ocean SST on seasonal timescales, and also may be involved in the interannual variability of the Asian monsoon by affecting heat content and SST anomalies as part of a biennial cycle of SST modulation (Loschnigg and Webster 2000). We will examine the cross-equatorial heat transport in a coupled model in this study to determine the relationship on interannual timescales to the monsoon, the IOZM, and the TBO.

W03 attempted to understand the Indian Ocean and monsoon phenomena described earlier, and the influence of ENSO, in terms of a single phenomena. They hypothesized that the IOZM and the TBO were integral parts of a self-regulation process of the monsoon that acted as negative feedbacks to keep the variability of the monsoon, both on annual and interannual timescales, within rather narrow limits. Their hypothesis resulted from the observation that the interannual variability of south Asian monsoon rainfall had a very small amplitude and that prolonged periods of drought or flood (multiyear) were extremely rare. The elements of the theory can be described as follows:

1) A strong (weak) monsoon year is accompanied by stronger southward (northward) meridional oceanic heat fluxes that tend to decrease (increase) the cross-equatorial SST gradient. These variations in meridional heat flux result from enhancements (decreases) in cross-equatorial Ekman transports of heat induced by the anomalous wind (Loschnigg and Webster 2000). It is noted that the anomalous ocean fluxes of heat are in the opposite sense to the anomalous

divergent wind component and the anomalous meridional atmospheric heat flux (W03). These anomalous oceanic heat transports are central to the biennial nature of Indian Ocean SSTs and the monsoon by producing for the following year a cooler or warmer north Indian Ocean regime, as originally suggested by Meehl (1994) and Meehl (1997).

2) The anomalous low-tropospheric monsoon wind induces anomalous upwelling in the eastern and the western parts of the ocean basin. A strong monsoon increases upwelling along the Somalia coast and Arabian Sea but reduces the upwelling along the coast of Sumatra. A weak monsoon, on the other hand, reduces the upwelling along the Somalia coast but increases it off Sumatra. Thus, a strong monsoon is associated with a west-to-east anomalous SST gradient, while a weak monsoon is associated with a reversed anomalous SST gradient. The creation of the anomalous SST gradient occurs in early summer at the time of minimal east–west SST gradient along the equator. It is hypothesized that the slack climatological SST gradient allows the positive feedback between the atmosphere and ocean and the growth of the IOZM, as suggested by Webster et al. (1999). Thus, the positive phase of the IOZM (warm western Indian Ocean) follows a weak monsoon while the negative phase follows a strong monsoon. It should be noted that these observations are in keeping with Saji et al. (1999) who noted that the IOZM was phase-locked to the annual cycle. W03 suggest that the anomalous heat flux associated with the IOZM emphasizes the biennial heat transports noted in (1) earlier.
3) The combined effects of the biennial Ekman meridional and zonal IOZM heat transports was to repress large-scale variations in monsoon magnitude. Furthermore, they suggested that these phenomena, in combination, would reduce the impact of external forcing of the monsoon, such as by ENSO. In fact, these regulation feedback processes occur relative to any major perturbation of the monsoon, which is why the development of the IOZM occurs sometimes in the absence of an extreme in ENSO. In this manner, anomalous meridional oceanic heat transports and the IOZM are natural responses of the perturbed monsoon system to external forcing and act to reduce the impact of such forcing.

One of the problems with the theory just outlined is that it is the result of a combination of interpretation of reanalysis results and other observations and experiments with stand-alone ocean models. A major purpose of this study is to examine the hypothesis and test its consistency from the context of a coupled ocean–atmosphere model.

In section 2 we will discuss the coupled model and the observational datasets used for comparison. Section 3 will assess the ability of the coupled model to simulate the biennial cycle in the Indian–Pacific Ocean region, and will discuss the role of the IOZM and the oceanic meridional heat transports in the Asian–monsoon ENSO system. Discussion and conclusions will be given in section 4.

2. Model description and comparisons with observational climatology

The model used is the NCAR CSM global coupled ocean–atmosphere–land surface–sea ice model, described in Boville and Gent (1998). The atmosphere used is the NCAR Community Climate Model 3 (CCM3) with T42 resolution and 18 vertical levels (Kiehl et al. 1998). The ocean component is a global GCM with a $2.4^\circ \times 2.4^\circ$ resolution, which is reduced to 1.2° latitude in the equatorial Tropics (Gent et al. 1998). The model also includes active land surface (Bonan 1998) and sea ice (Weatherly et al. 1998) components. The coupled model is run without flux adjustments. For this study we analyze monthly mean fields of the first 100 yr of the 300 yr control run. The oceanic fields are available only from year 27 onward, as the implementation of the model code for the calculation of the monthly mean fields was not available before that period of the model control run.

Meehl and Arblaster (1998) discuss the ability of the CSM to reproduce characteristics of ENSO and the Asian–Australian monsoon. They find that the CSM is able to reproduce the major features of the monsoon system, including the mean climatology, interannual variability, and the connections of the Asian–Australian monsoon to the tropical Pacific. The model adequately simulates the seasonal cycle of SSTs in the eastern equatorial Pacific, as well a consistent Bjerknes response. Time series of the Niño-3 (5°N–5°S, 90°–150°W) SST anomaly index in the CSM produces an amplitude of about 60% of the observed variability, within the range simulated by other coupled models. Meehl and Arblaster (1998) find that spectra for the model time series of Niño-3 SST show a significant peak in the ENSO periods (3–5 yr), with smaller peaks in the TBO (2–3 yr) and decadal periods. They also note that the model cold tongue in the Pacific extends too far west as compared to observations (similar to other coupled models), which contributes to shifting the ascending branch of the Walker circulation further westward. This results in a slightly weaker association of central and eastern Pacific SST anomalies with the Australian monsoon, and a stronger association with the Indian monsoon. As in observations, indices of both Asian and Australian monsoon strength are negatively correlated with Niño-3 SST, and both indices show amplitude peaks in the ENSO and TBO frequencies (3–6 yr and 2–3 yr, respectively). In terms of simulating the observed ENSO–monsoon relationships, a comparable coupled model (Arblaster et al. 2002) and the atmospheric component of the CSM run with SST anomalies (Meehl and Arblaster 2002a)

both successfully simulate the general features of the interactions between the Pacific and Indian Oceans. Meehl and Arblaster (1998) also note that the model has a tendency to produce multiyear ENSO events. Although these types of protracted events have been noted in observations (Trenberth and Hoar 1996; Allan and D'Arrigo 1999; Reason et al. 2000), their existence in the model solutions influences the biennial tendency of the results, and will be discussed further in section 3.

Comparisons of the model climatology for precipitation, surface skin temperature (T_s) and 850-mb winds with the Xie and Arkin (1996) CMAP precipitation dataset and the (National Centers for Environmental Protection) NCEP–NCAR reanalysis dataset (Kalnay et al. 1996) are shown in Figs. 1 and 2. The precipitation in the CSM (Fig. 1) is higher than in the observation for the regions in the equatorial Indian Ocean and in the Pacific warm pool region near the Phillipines by up to 6 mm day^{-1}. The precipitation errors in the CSM are related to errors in the SST fields via differences in latent heat flux, evaporation, and low-level winds, leading to differences in the low-level moisture convergence, especially in the Phillipine region in June–September (JJAS; Fig. 1c). Latent heat flux in the North Indian Ocean and western Pacific ITCZ regions is about 30–60 W m^{-2} too great, resulting in evaporation errors of between 1–2 mm day^{-1} too high. The enhanced convection associated with the large precipitation errors in the equatorial regions of the Indian Ocean may lead to enhanced circulation variability in the model as compared to observations. This would affect the east–west circulation and thus may be associated with the westward shift of the Walker cell noted earlier. Despite these errors, Meehl and Arblaster (1998) show that, overall, relationships and coupled interactions are comparable to observations especially in the central and western Indian Ocean. Sensitivity experiments with different Indian Ocean SST anomalies (Meehl and Arblaster 2002a) show the importance of equatorial Indian Ocean SST anomalies and the ability of the atmospheric model to simulate the associated wind forcing. This gives confidence that the interactions are reasonably well represented in the coupled model. Figure 2 shows surface temperatures in the CSM in the Indian Ocean and western Pacific warm pool regions about 1°C cooler than NCEP reanalysis values in many regions throughout the year, and a monsoon inflow in JJAS that is weaker than in observations (Fig. 2c), resulting in reduced summer monsoon rainfall in the Indian region, particularly in the Bay of Bengal region (Fig. 1c). There also exist significant errors in precipitation in the CSM when compared to observations for the boreal fall and winter seasons. In September–November (SON) and December–February (DJF), the CSM shows higher precipitation than the observations in the western equatorial Indian Ocean (Figs. 1e,g). These errors in convection could affect the equatorial response of the atmosphere and thus the mechanisms associated with the IOZM. The model equatorial westerlies are stronger than those of observations in March–May (MAM) (Fig. 2a). The model generally has stronger inflow into the Indonesian region from both the Indian and Pacific Oceans as compared to observations. This relates to issues involved with the overextensive cold tongue regime mentioned earlier and the westward shift of the Walker circulation. The dynamical feedbacks result in latent heat flux anomalies, upwelling, and strong low-level moisture convergence leading to excessive precipitation in some areas. In general, for coupled interactions, this leads to enhanced ''coupling strength'' (see Zebiak and Cane 1987) and enhanced coupled variability in the Indian Ocean, which facilitates the elucidation of the mechanisms that will be studied in this paper.

Gent et al. (1998) find the model Indonesian Throughflow (ITF) to have an average value of 16.7 Sv (1 Sv $\equiv 10^6$ m^3 s^{-1}), which is within the range of observational estimates, although they note the CSM model value might be a little high. They also note that the Indonesian passage has been artificially widened, since the model cannot resolve the islands in the archipelago region. The role of the Indonesian Throughflow in affecting the processes in this region is not analyzed in this paper, as it is such a large and separate issue with its own set of processes and uncertainties in observations and in models that it is beyond the scope of the present study. We intend to include an analysis on the role of the ITF and its role in the interannual variability of Indian Ocean dynamics in a future study.

Aside from the previously mentioned differences as compared to observations, the model does a reasonable job in simulating the large-scale aspects of the annual cycle of the Asian–Pacific region, and is therefore sufficient for the purposes of this paper.

3. Results

a. Analysis of local and remote TBO forcings

In this section we analyze the ability of the CSM to simulate the various local and remote forcings during the boreal spring transition period of the TBO, as well as the ability of the CSM to transition from the boreal summer Asian monsoon to the boreal winter Australian monsoon. We first perform lagged singular value decomposition (SVD) analysis to define the maximum covariability of the spatial associations between various fields in the boreal spring season (MAM) and the resulting Indian summer (JJAS) monsoon precipitation. The analysis is similar to the observational study of Meehl and Arblaster (2002b), to which we will be comparing our results. We focus on three main local and remote processes that are known to influence the interannual variability of the Asian summer monsoon (Meehl and Arblaster 2002b). First, SST anomalies in the Indian Ocean can affect the Indian summer monsoon moisture source and produce a more vigorous monsoon circulation. Second, SST anom-

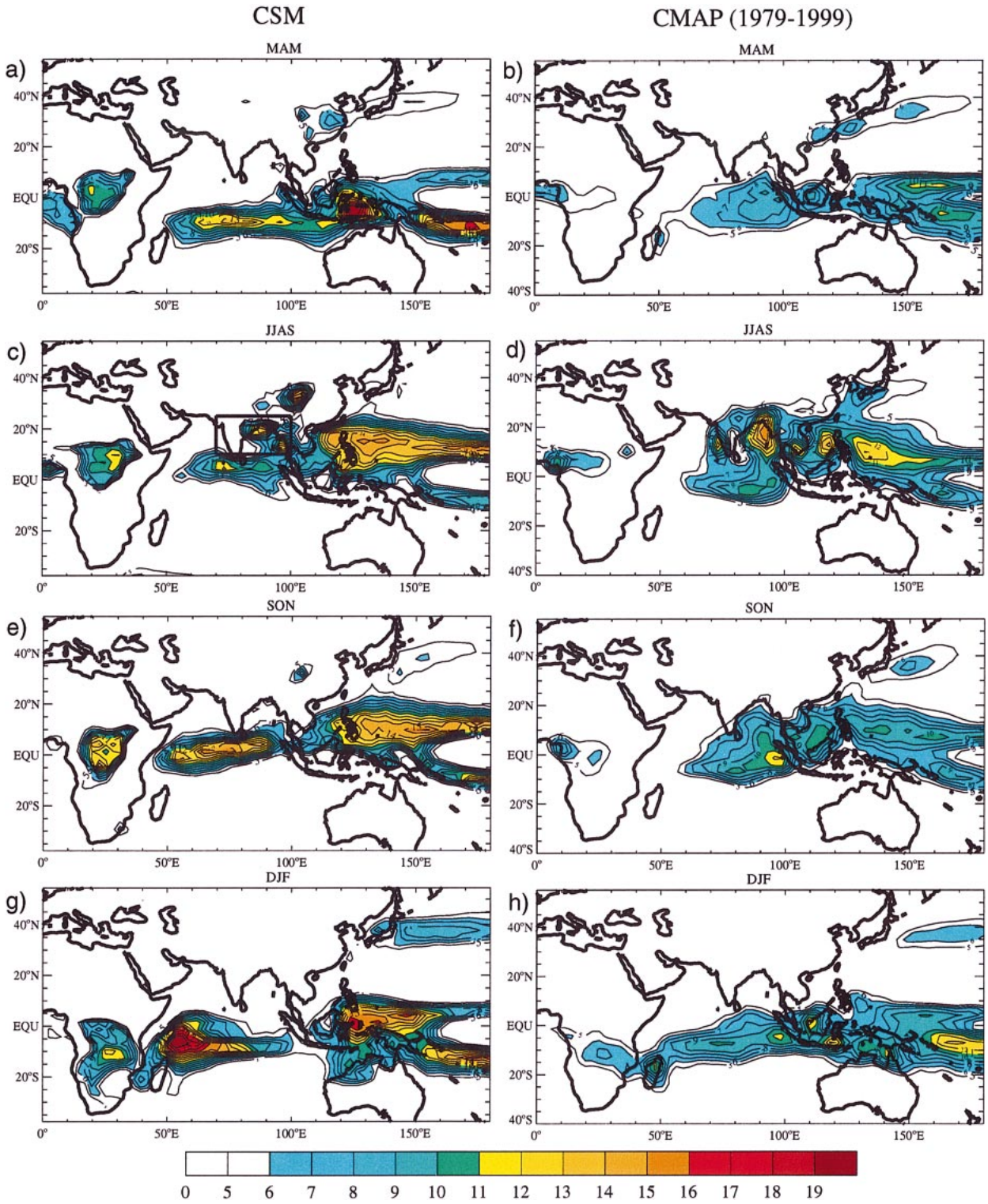

FIG. 1. (a)–(h) Model and observational climatological mean precipitation (mm day^{-1}) for MAM, JJAS, SON, and DJF. Boxed area shown in (c) is the region used for the calculation of the CI1 precipitation index (10°–25°N, 70°–100°E).

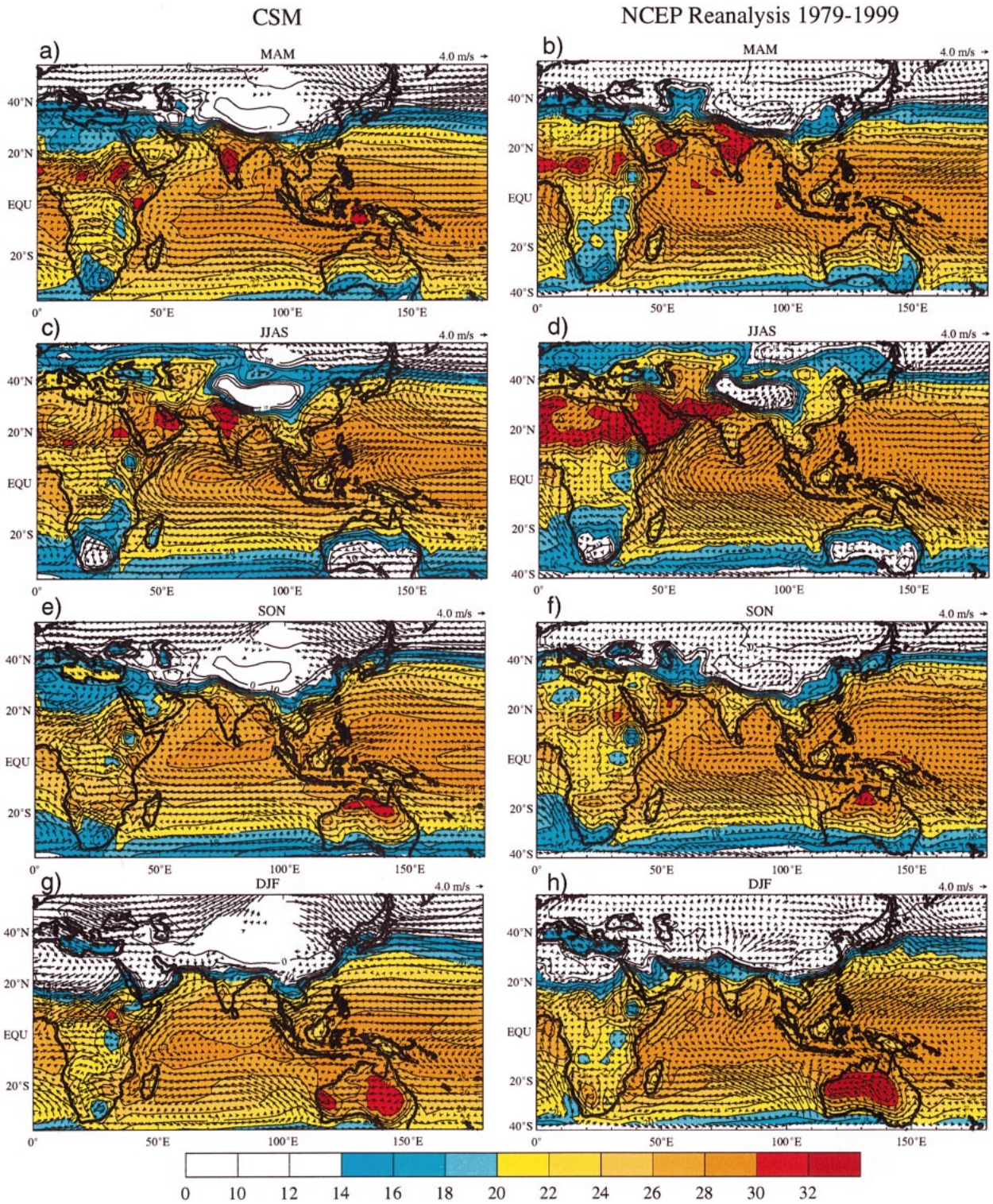

FIG. 2. Model and reanalysis climatological mean surface skin temperature (T_s, in °C) and 850-mb winds (m s^{-1}) for MAM, JJAS, SON, and DJF.

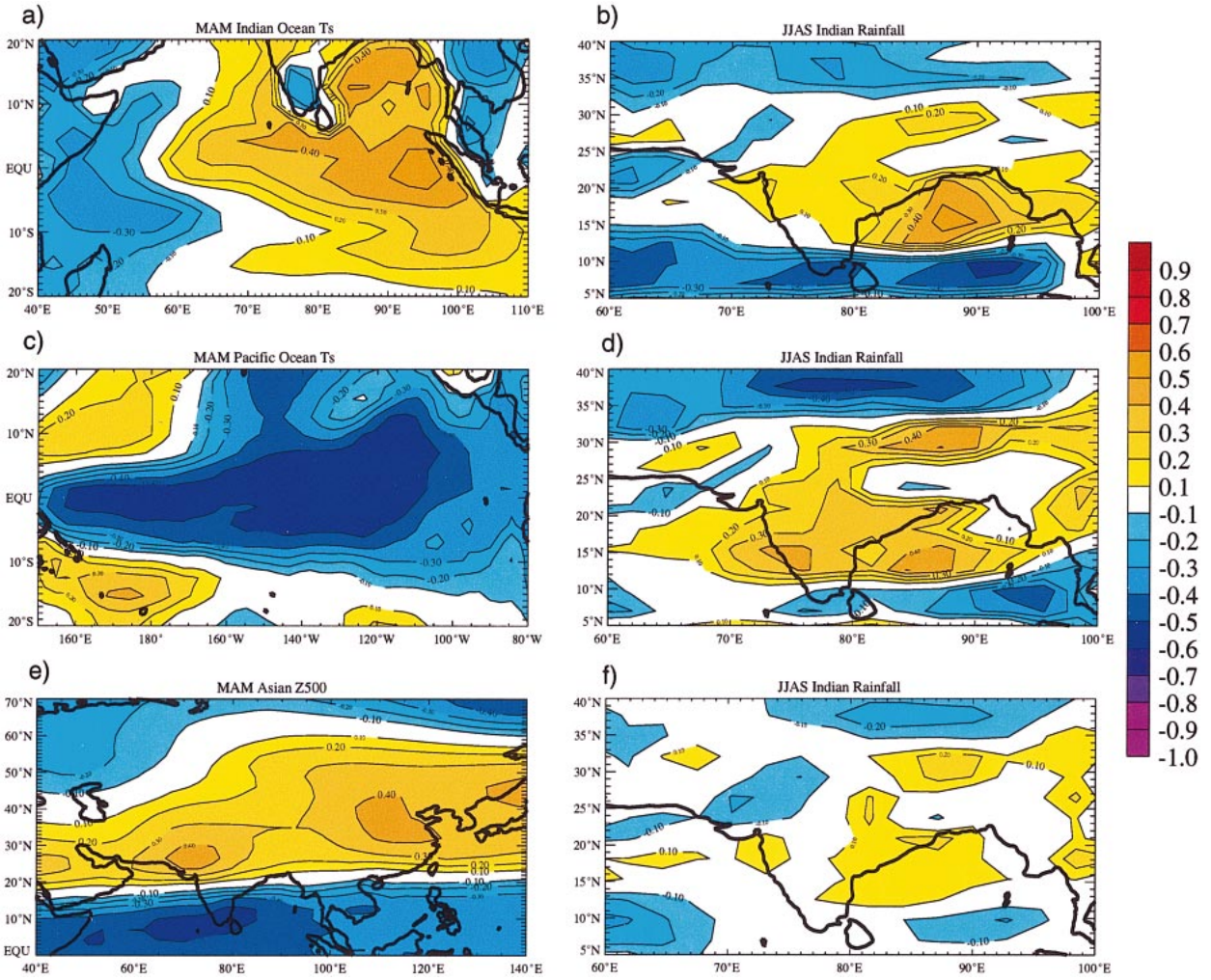

FIG. 3. First component SVD correlation patterns, relating (a) MAM Indian Ocean T_s (20°S–20°N, 20°–110°E) to (b) JJAS Indian rainfall (5°–40°N, 60°–110°E); (c) MAM Pacific Ocean T_s (20°S–20°N, 150°E–80°W) to (d) JJAS Indian rainfall; (e) Asian 500-mb height (30°–70°N, 50°–110°E) to (f) JJAS Indian rainfall. Note the correlations in (a), (c), and (e) extend beyond the ares used in the SVD calculation.

alies in the central and eastern Pacific Ocean can affect the monsoon through changes in the large-scale east–west Walker circulation. And third, the 500-hPa height anomalies over Asia cause changes in the large-scale atmospheric circulation, which result in changes in Asian land temperatures that enhance the land–sea temperature gradient that drives the Indian summer monsoon. The association of each of these three forcings in the model are shown in Fig. 3.

For positive T_s anomalies in the central and eastern Indian Ocean in MAM (Fig. 3a) there are positive precipitation anomalies located mainly in the Bay of Bengal, but also over the central and northern Indian subcontinent in JJAS (Fig. 3b). Increased T_s in these areas provides the Indian summer monsoon with an added moisture source and helps influence the increased strength of the monsoon circulation. Compared to observational results (Meehl and Arblaster 2001), the model produces a similar strong response of T_s over the central Indian Ocean but fails to produce the precipitation response in JJAS over western India, producing increased values only over eastern India and the Bay of Bengal. This result is likely related to similar systematic errors in the CSM climatology as noted in section 2. Negative T_s anomalies in the central Pacific Ocean in MAM (Fig. 3c) are associated with positive rainfall anomalies over much of India and the Bay of Bengal in JJAS (Fig. 3d). The relationship between the precipitation anomalies over India and the T_s anomalies in the Pacific is the result of changes in the large-scale east–west circulation spanning the Pacific and Indian Oceans, which affect the monsoon through either enhancing or suppressing the vertical motion of the monsoon circulation over the Indian subcontinent, as seen in observations by Meehl and Arblaster (2002b). Results from that observational study show that during the biennial cycle the sign of the SST anomaly in the central and eastern Pacific Ocean transitions from positive anom-

alies in MAM to negative anomalies in JJAS, leading to increased precipitation over the Indian region in JJAS. The model result shows persistent negative anomalies, starting in MAM and continuing through the boreal summer months (not shown). The continuous La Niña-like conditions still produce positive rainfall anomalies in JJAS. The persistent T_s anomalies of one sign is an illustration of the tendency for the model to produce multiyear ENSO events. For positive 500-hPa height anomalies over central and south Asia in MAM (Fig. 3e), there are small positive precipitation anomalies in eastern India and the Bay of Bengal. Meehl (1997) suggests that this pattern is a Rossby wave response to convective heating anomalies over the equatorial Indian Ocean and western Pacific in the form of an anomalous ridge in central Asia. The results here show a slightly weaker precipitation response over India and the Bay of Bengal as compared to observations, but otherwise a similar response over India and the monsoon to the Asian temperature anomalies. Negative precipitation anomalies exist to some degree between 5°–15°N in Figs. 3b,d,f. These negative anomalies are most pronounced for the Indian and Pacific T_s SVDs, and weakly evident for the 500-hPa height SVD. This signifies a northward shift of the precipitation maximum for this covariability pattern, with positive values over south Asia and more negative values just south of India.

It is possible to quantify the impact of each of these local and remote forcing mechanisms on the monsoon precipitation so as to assess the relative strength of each of the mechanisms in each year, and whether they are functioning independently from one another or whether they are acting in unison. We analyze spatial anomaly pattern correlations (Lau and Wu 1999; Meehl and Arblaster 2001) between the model-produced summer monsoon rainfall and the SVD projections produced individually and cumulatively. The cumulative pattern correlation for the *k*th SVD for *i* transition conditions to the model-produced precipitation anomaly for the *j*th year is

$$A_{i,j} = \left\langle O_j \sum_{k=1}^{i} S(k)C(k)_j \right\rangle,$$

where $\langle\ \rangle$ is the spatial anomaly pattern correlation over the monsoon region, S is a normalized precipitation SVD pattern for JJAS associated with a MAM forcing mechanism, C is the precipitation SVD expansion coefficient for that year, and O is the model-produced Indian rainfall anomaly. Each anomaly pattern correlation is first calculated separately (Fig. 4a), and then in a cumulative form (Fig. 4b). From Fig. 4a it is seen that in many years all three mechanisms are acting in unison to produce variations in Indian summer monsoon rainfall, and in some years all three mechanisms are failing to have much of an effect on the precipitation. For a majority of the years, the three conditions are very similar in their strength of correlations, and then fall out of synchronous impacts during certain decades when all three are continuously weak (e.g., years 30–40 and 60–70). This is indicative of the decadal variability in the relationships, and is also apparent in observations (Torrence and Webster 1998). The cumulative pattern correlation shown in Fig. 4b also includes periods of especially strong relationships (e.g., years 10–15, 20–30, and 50–60). The mean cumulative anomaly pattern correlation for the 100 yr of model output is 0.46. When we use the reconstructed SVD patterns to calculate the Indian summer monsoon rainfall index, that index correlates to the actual precipitation index at 0.8, which is slightly lower than that of the observational study (0.9), but high enough to illustrate the model's ability to reproduce the correct forcings for this region.

Between the boreal summer and winter monsoons in the Asian–Australian monsoon region, there tends to be a persistence between the transition from a strong Indian monsoon to a strong Australian monsoon, with a convective maximum progressing over Southeast Asia in SON towards north Australia in DJF (Webster et al. 1998; Meehl and Arblaster 2002b). For this reason we undertake a similar analysis for the boreal winter Australian monsoon, using the SON conditions as the forcing mechanisms for the DJF precipitation over northern Australia. Three processes thought to be associated with the Australian monsoon are: first, SST over the equatorial and southern Indian Ocean; second, SST anomalies over the central and eastern Pacific Ocean; and third, rainfall over Southeast Asia, which is a signal of the transition of the area of maximum convection from south Asia during JJAS to northern Australia in DJF (Meehl and Arblaster 2002b).

Results for the SVD analysis of SON forcings on DJF rainfall over northern Australia are shown in Fig. 5. The general pattern of T_s anomalies is a dipole pattern of warm eastern equatorial and southeast Indian Ocean temperatures, and cooler temperatures in the western equatorial and Arabian Sea regions in SON (Fig. 5a) associated with stronger precipitation over northern Australia and the Maritime Continent in DJF (Fig. 5b). In the Pacific Ocean, cooler temperatures in the central equatorial basin (Fig. 5c) are associated with slightly higher precipitation for similar regions over northern Australia and the Maritime Continent in DJF (Fig. 5d), but of slightly lower strength. Finally, the transition of the convective maximum in SON over Southeast Asia and the Maritime Continent (Fig. 5e) is associated with increased precipitation over the regions near northern Australia (Fig. 5f). Except for some slight differences in the strength of the correlations, these patterns are very similar to those of observations (Meehl and Arblaster 2002b). The pattern correlations for DJF rainfall are shown in Fig. 6. The striking feature is how all three of the individual pattern correlations follow each other very closely (Fig. 6a), showing how the different forcing mechanisms are closely connected to each other in their ability to determine boreal winter Australian monsoon

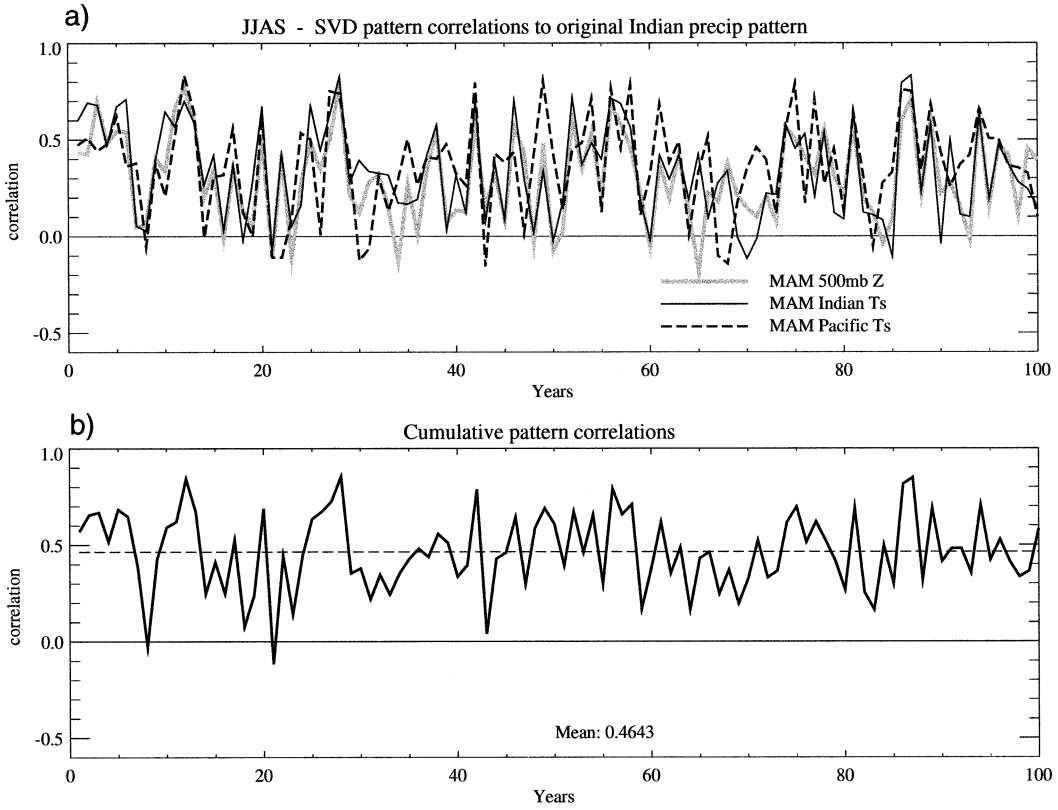

FIG. 4. (a) Time series of individual anomaly pattern correlations for the MAM SVD patterns of Indian Ocean T_s (solid black line), Pacific Ocean T_s (dashed black line), and Asian 500-mb height (solid gray line) with the JJAS Indian rainfall. (b) Cumulative anomaly pattern correlation for all three patterns in (a). Dashed line shows the mean correlation of 0.46.

precipitation. This close association of the three major forcing mechanisms was also seen in observations by Meehl and Arblaster (2002b), who find that once the TBO transition is complete in MAM, there is greater seasonal persistence from JJAS to SON to DJF, from the Indian to the Australian monsoon. The mean cumulative anomaly pattern correlation for the Australian monsoon transition conditions in Fig. 6 is 0.43.

The similarity of the model results shown here to those of observations (Meehl and Arblaster 2002b; MAL), suggests that the model accurately simulates the dynamics inherent in the interannual variability of this region, and that the correlations and connections presented imply causality through a consistent set of interconnected physical processes. From the previous analysis we can conclude that the coupled model sufficiently reproduces the observed local and remote forcing mechanisms that affect anomalous rainfall in both the summer and winter phases of the Asian–Australian monsoon, as well as the transition from a strong summer to winter monsoon. For this reason, we will use the model to diagnose the relationship of the coupled ocean–atmosphere dynamics in the Indian Ocean with the large-scale anomalies of the Asian–Australian monsoon, and examine how they play a role in the TBO and the Indian–Pacific Ocean climate.

b. The IOZM and Indian–Pacific Ocean relationships in the CSM

To analyze the IOZM in the model, we produce an index which is similar to the ''dipole mode index'' (DMI) of Saji et al. (1999). The index is calculated as the difference of the surface temperature anomalies between the western (5°S–10°N and 40°–55°E) and the eastern equatorial Indian Ocean (10°S–5°N, 90°–102°E). Figure 7 shows the monthly values of the DMI and the means for the boreal fall season (SON) for the 100 yr of the model control run. A power spectrum of the monthly DMI shows significant peaks in the 2–3-yr range, and smaller peaks in the 3–5-yr range (not shown). When seasonal composites of T_s and 850-mb winds are taken for years when the SON DMI is above and below one standard deviation (Figs. 7c–e), a pattern emerges which closely resembles that of observational studies (Webster et al. 1999; Saji et al. 1999), with strong temperature anomalies of one sign near the eastern equatorial Indian Ocean regions, and opposite sign

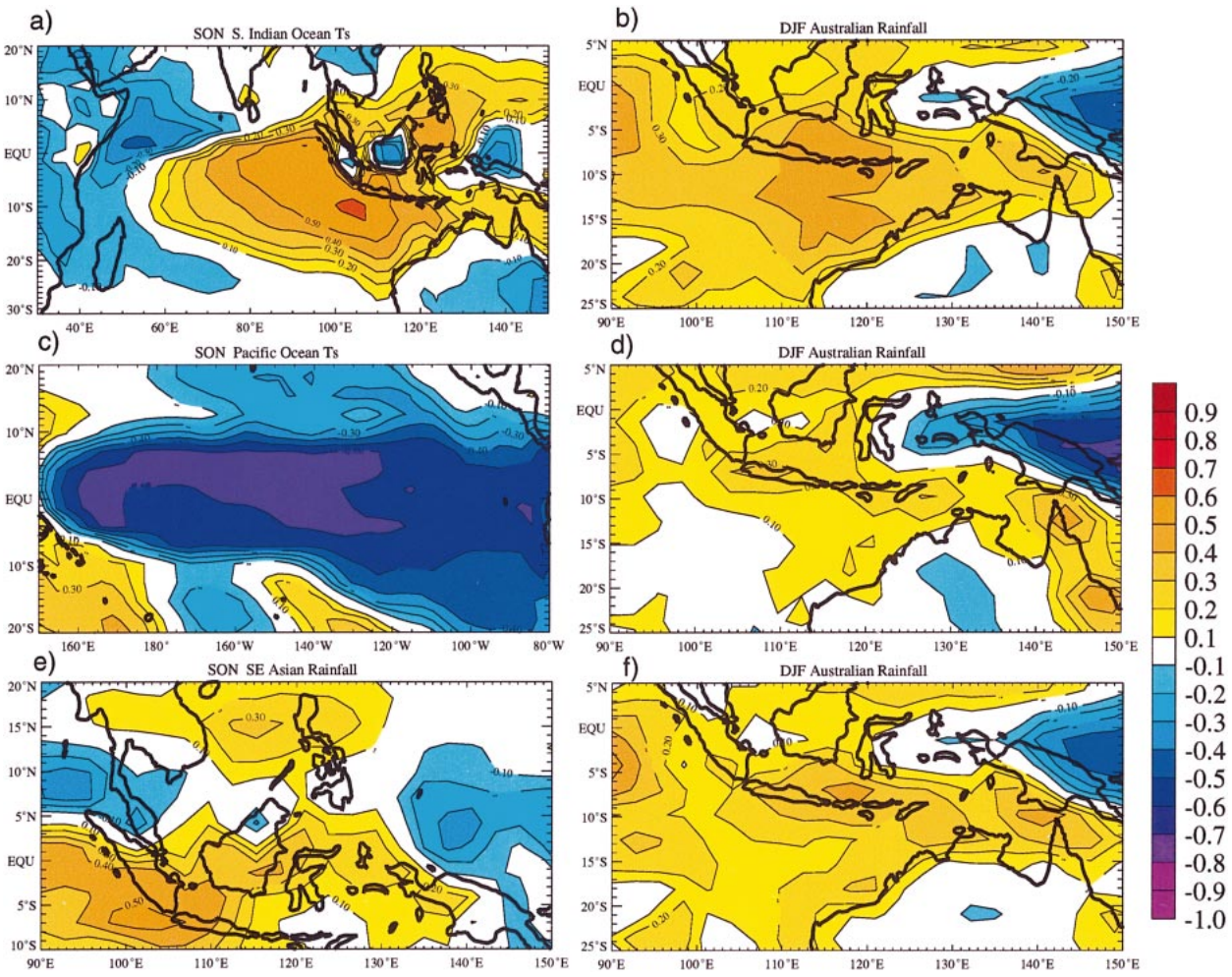

FIG. 5. First component SVD correlation patterns, relating (a) SON southern Indian Ocean T_s (25°S–0°, 90°–120°E) to (b) DJF Australian rainfall (20°S–5°N, 100°–150°E); (c) SON Pacific Ocean T_s (20°S–20°N, 150°E–80°W) to (d) DJF Australian rainfall; (e) SON southeast Asian rainfall (10°S–10°N, 90°–130°E) to (f) DJF Australian rainfall.

anomalies in a horseshoe pattern in the western part of the basin. Note that Figs. 7c–e are composites of ''negative'' minus ''positive'' IOZM years, so as to correspond to the TBO composites in the following sections. For comparison, 1997 was a positive IOZM year, with warm SST anomalies in the western equatorial Indian Ocean and cool in the east in September–October 1997, the opposite sign anomalies to those shown in Fig. 7d.

In terms of the general Indian Ocean response to ENSO in the model, T_s in the Niño-3.4 region correlates most strongly (0.3) to an index of basinwide T_s anomalies in the Indian Ocean (20°S–20°N, 50°–100°E) when the Niño-3.4 (5°N–5°S, 120°–170°W) index leads by 7 months (with each index smoothed by a 13-month running mean prior to analysis), which is a slightly longer lead and lower correlation than the observational results shown in Venzke et al. (2000). The spatial structure of the Indian Ocean T_s anomalies correlated to the Niño-3.4 index at this lag can be seen in Fig. 8, which shows a pattern consisting of a temperature gradient at the equator, with a narrow band of negative values in the eastern equatorial regions and a horseshoe-shaped pattern of positive values in the western part of the basin. This pattern is similar to the observational analysis of Xie et al. (2002, their Fig. 10). The narrow band of cold T_s anomalies suggests a Bjerknes-type feedback, with equatorial upwelling in a positive DMI year induced by the easterlies near the Sumatra coast.

c. Indices relating to monsoon strength

In this section we will analyze two indices relating to Asian summer monsoon strength that will be used in following sections to assess ocean dynamical features as they relate to the interannual variability of the Asian monsoon. The first is a boreal summer (JJAS) rainfall index which is similar to the all-India rainfall index of Parthasarathy et al. (1991), except that it includes rainfall over oceanic regions as well as land, which is important for determination of large-scale strength of the

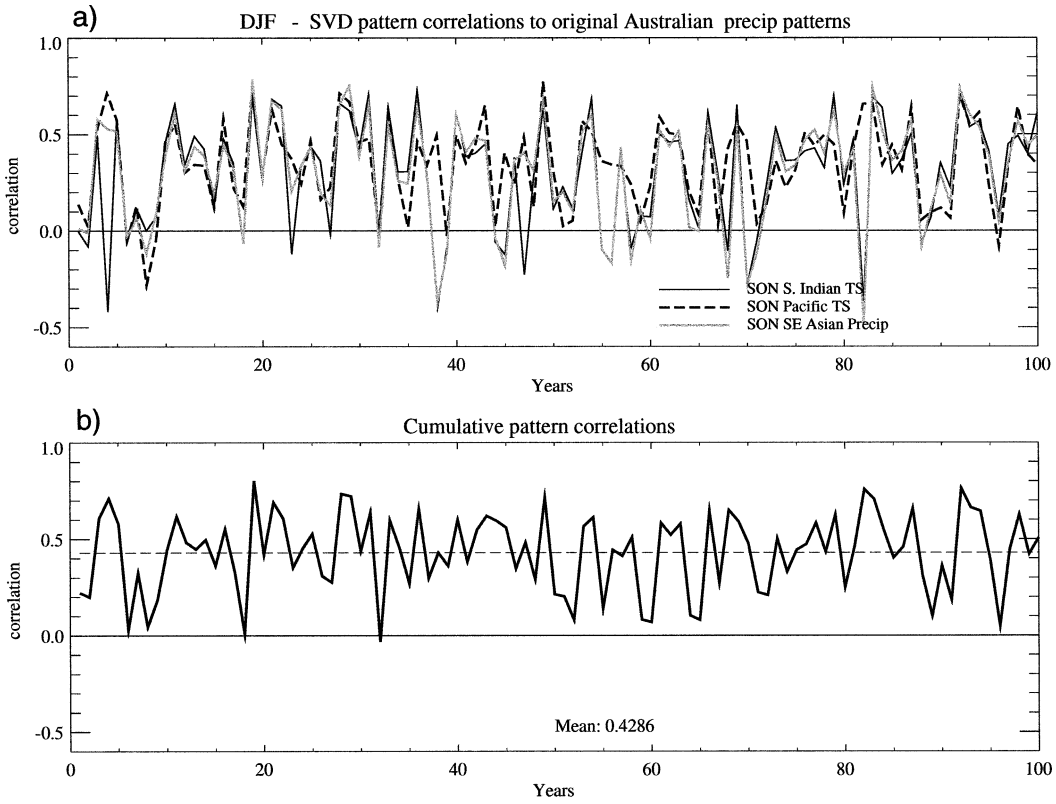

FIG. 6. (a) Time series of individual anomaly pattern correlations for the SON SVD patterns of Indian Ocean T_s (solid black line), Pacific Ocean T_s (dashed black line), and Southeast Asian rainfall (solid gray line) with the DJF Australian rainfall. (b) Cumulative anomaly pattern correlation for all three patterns in (a). Dashed line shows the mean correlation of 0.42.

monsoon. The boundaries for the rainfall index are shown in Fig. 1c (10°–25°N, 70°–100°E). This index area is similar to the boundaries of the convective index used by Wang and Fan (1999), and we will use the similar term CI1 to identify it.

Another method of determining the strength of the Asian summer monsoon is by the westerly wind shear (Webster and Yang 1992). Figure 9a shows the climatological 850–200-mb U wind shear ($U_{850} - U_{200}$) for JJAS, which is used for the calculation of the Westerly Shear Index (WSI1). Figure 9b shows the correlation of $U_{850} - U_{200}$ wind shear for JJAS with the CI1 for 100 yr of the model. These results are very similar to the observational analysis of Wang and Fan (1999, see their Fig. 4a), with strong positive values over the western Indian Ocean and eastern Africa between 20°N and 20°S. The region used for the calculation of the WSI1 (5°–15°N, 35°–75°E) is in the region of the highest positive correlation with the CI1 (+0.68), and is very similar to the region used in Wang and Fan (1999). Also interesting to note in Fig. 9b is the large region of negative correlations over the western Pacific Ocean, similar to observations, which is an illustration of the Walker circulation strength associated with ENSO–monsoon relationships. This is shown explicitly in schematic fashion in Meehl and Arblaster (2002b, their Fig. 3) and for omega vertical velocity representation for TBO composites in MAL (their Fig. 4).

The timeseries for the WSI1 and the CI1 are shown in Fig. 10a for the first 100 yr of the model control run. The dots representing the strong and weak TBO years will be discussed in the next section. Power spectra of the monthly values for the CI1 and WSI1 are shown in Figs. 10b and 10c, respectively. Both spectra show small peaks in the 2–3 yr range, signifying a signal in the TBO timescale. The WSI has some peaks in the 3–5-yr range, signifying some relationships to more longer-scale variability typically seen of ENSO-like Pacific Ocean variability. Although both spectra also show significant power in the decadal range, variability on this timescale will not be discussed in this paper.

d. Indian Ocean dynamics and the TBO

To analyze the relationship of Indian Ocean dynamics to the TBO and to the interannual variability of the monsoon, we construct composites from the model based on years where both of the indices described in the previous section (CI1 and WSI1) are relatively greater or less than the previous or following years. That is,

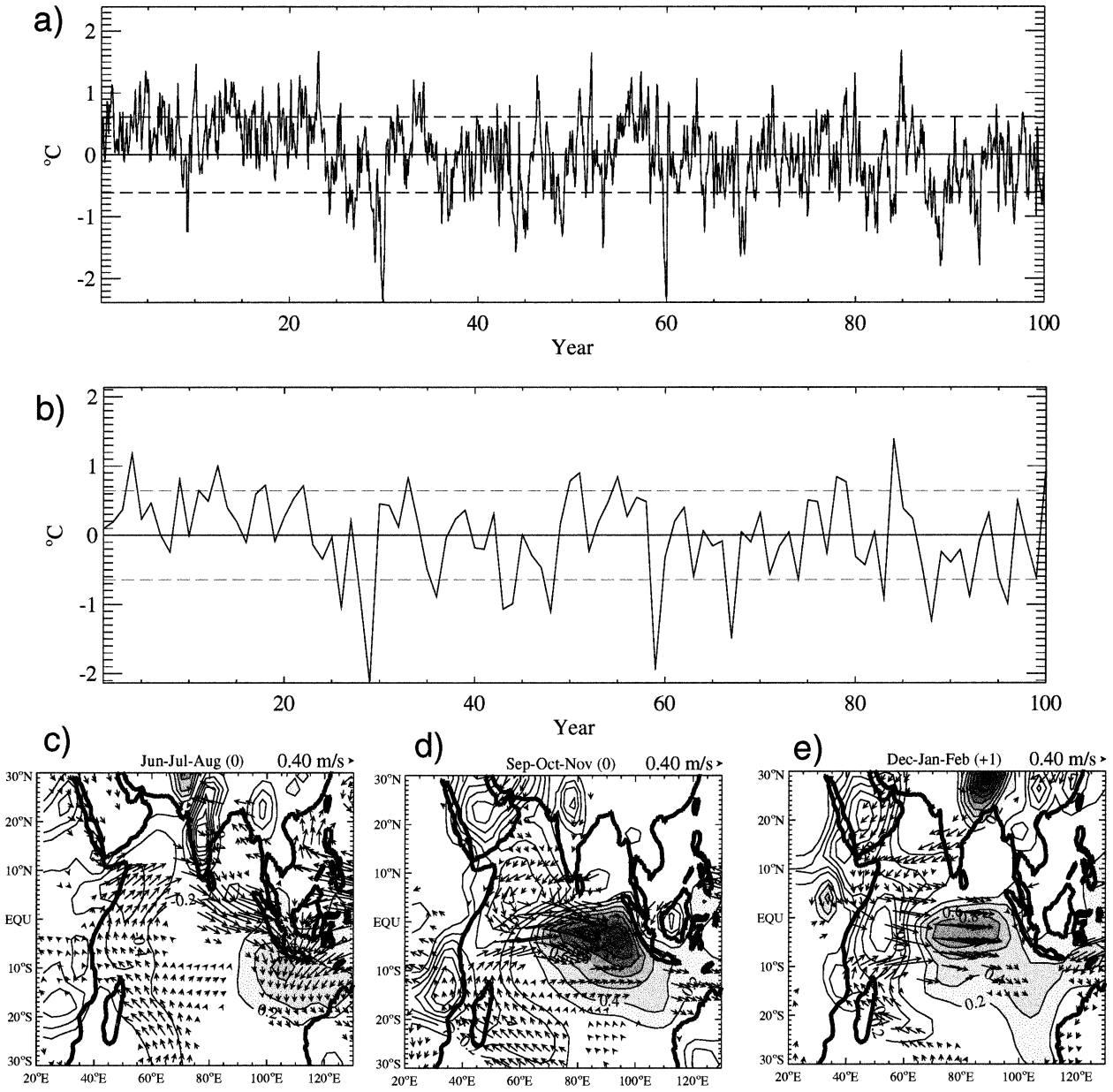

FIG. 7. (a) Time series of the DMI (T_s anomalies from 5°S–10°N, 40°–55°E minus 10°S–5°N, 90°–102°E). Dashed lines are $\pm 1\ \sigma$ levels. (b) Time series of the SON DMI. Composite T_s and 850-mb wind anomalies for negative minus positive IOZM years, as measured by years that the SON DMI is $\pm 1\ \sigma$ levels, for (c) JJA(0), (d) SON(0), and (e) DJF(+1). Contour level is 0.2°C, with the zero level contour omitted. Positive regions above +0.2°C are shaded. Only values above the 95% significance level are plotted.

if P_i is the value of the index (both CI1 and WSI1 in this case) for a given year i, then a relatively strong year is defined as

$$P_{i-1} < P_i > P_{i+1}$$

and a relatively weak monsoon is defined as

$$P_{i-1} > P_i < P_{i+1}.$$

Such strong and weak years are defined as ''biennial'' years (Meehl and Arblaster 2002b). These years are shown in Fig. 10a as the solid dots. All composites shown in this section will be for strong minus weak years. Note that the results shown below do not change appreciably when calculating the composites based on years when the indices are above or below one standard deviation (for either the precipitation index or the westerly shear index). The major difference in the results is a slightly stronger signal of the multiyear events (of both ENSO and monsoon), and thus a weaker transition to anomalies from one sign to the other in the boreal spring season.

Figure 11 shows the composites for T_s and 850-mb

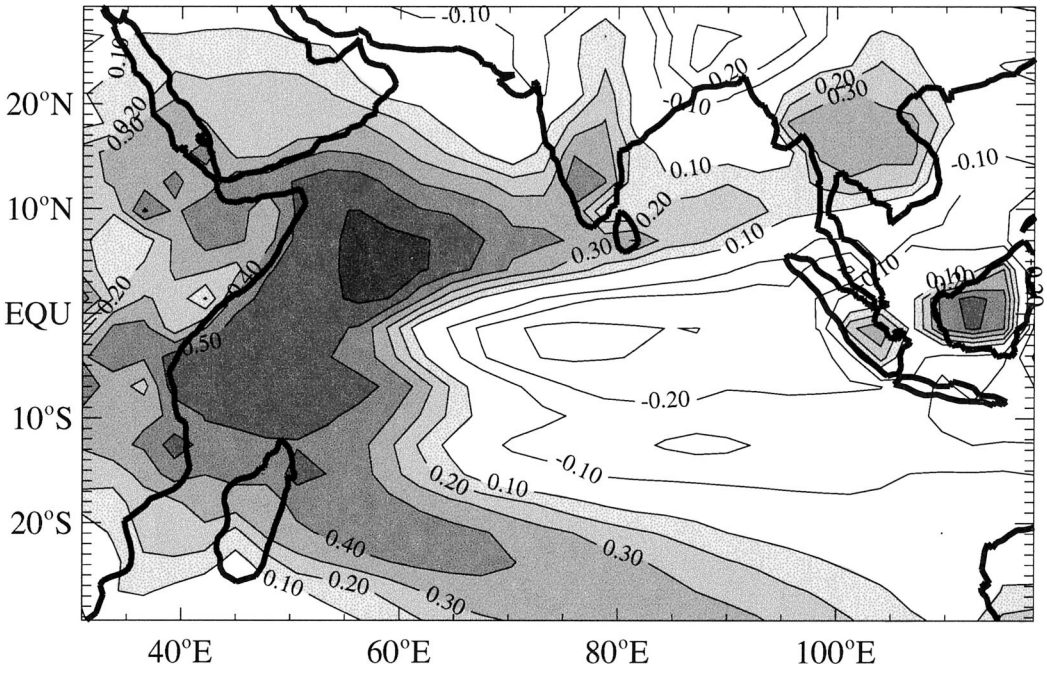

FIG. 8. Spatial distribution of the correlation coefficients of the Indian Ocean T_s anomalies with the Niño-3.4 T_s anomalies at a lag of 7 months, with the Niño-3.4 leading. Data were smoothed using a 13-month running mean prior to the analysis. Contour level is 0.1, with the zero level contour omitted. Regions of positive correlation above +0.1 are shaded.

winds for six seasons from the model during part of a biennial cycle [MAM(0), JJA(0), SON(0), DJF(+1), MAM(+1), and JJA(+1); JJA(0) is the season for which the composites are based]. The strong monsoon circulation is seen in JJA(0) (Fig. 11b), with strong southeasterlies in the southwestern Indian Ocean and strong alongshore winds near Somalia. There are also northwesterlies near Sumatra, which are an indication of reduced alongshore and offshore winds there. Also during this season, the regions around northwest and western Australia are dominated by anomalously strong northwesterlies, seen in similar TBO composites for observations in MAL. They show strong convection that stretches across the tropical Indian Ocean, which is associated with small-amplitude southeasterly anomaly surface winds in the southwestern Indian Ocean, and northwesterly anomaly surface winds north of Australia not unlike that seen for the model composites in Fig. 11b. These surface wind anomalies in the observations and the model are consistent with precipitation anomalies shown later. The anomalous northwesterlies extend somewhat farther south and west in the model composites as compared to observations, not surprising given the documented systematic error in the model involving the westward-shifted Walker circulation.

Surface temperatures over the Indian subcontinent are anomalously cool in JJA(0) and SON(0) (Fig. 11c) from increased monsoon precipitation and wetter land surfaces. During the period near JJA(0), the central and eastern Pacific Ocean transitions to cool surface temperatures. These cool anomalies, along with the strong easterly winds near the western equatorial regions in the Pacific Ocean area in JJA(0) and SON(0) have the sign of La Niña conditions. This pattern of T_s anomalies in the Pacific Ocean is consistent with the SVD analysis in Fig. 5c. The development of a negative (cool west, warm east) dipole of surface temperature in the equatorial Indian Ocean region begins in SON(0), which is consistent with the SVD analysis in Fig. 5a. The cool western Indian Ocean has contributions from anomalously strong upwelling from the strong alongshore monsoon winds. The cooling from vertical mixing is in addition to the influence of horizontal mixing, latent heat fluxes, and equatorial waves (Murtugudde et al. 2000). The warm anomalies in the eastern equatorial regions are partly a consequence of the reduced upwelling there due to the weaker alongshore and offshore winds near Sumatra. The surface winds are westerly along the equator in the Indian Ocean during SON(0) and DJF(+1) (Fig. 11d). This situation can be thought of as a negative SST dipole, and is the reversed sign of the positive SST dipole event of 1997/98 (Webster et al. 1999), which had an anomalously warm western equatorial Indian Ocean and cool eastern equatorial regions. The cool temperatures persist into DJF(+1) and MAM(+1) in the western Indian Ocean (Figs. 11d,e), which is a remnant of the previous strong monsoon. In the Pacific Ocean, there is the development of warm surface temperature anomalies in the central and eastern part of the equatorial regions in JJA(+1) (Fig. 11f), such

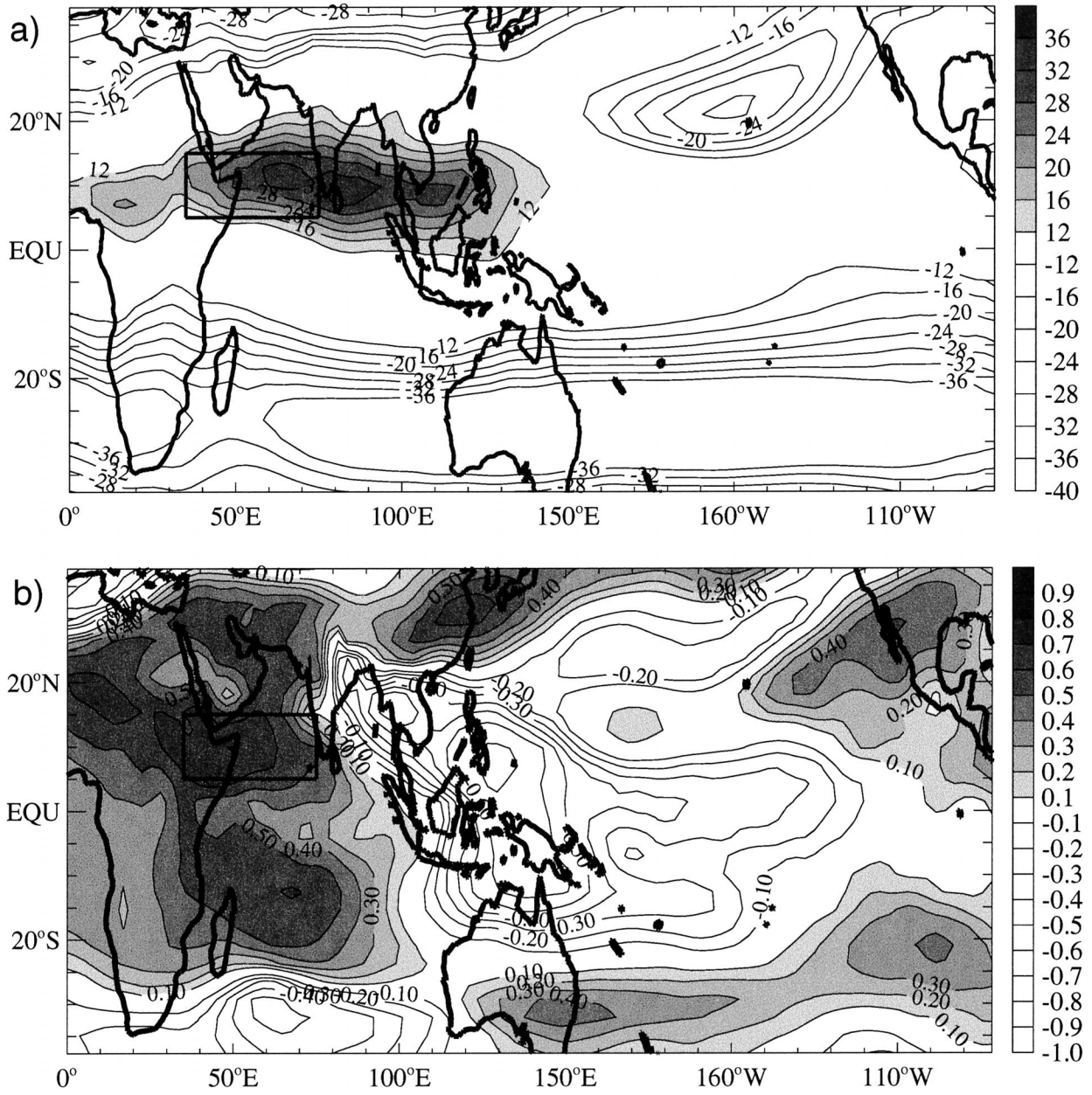

FIG. 9. (a) Model climatological $U_{850} - U_{200}$ shear for JJAS (m s^{-1}); positive regions above 12 m s^{-1} are shaded. (b) Correlation of model CI1 to $U_{850} - U_{200}$ shear for JJAS; positive regions above 0.1 are shaded. Boxed area in both (a) and (b) shows the region used for the calculation of the WSI1 *U*-shear index (5°–15°N, 35°–75°E).

as that seen in El Niño events. There are also signs of a weaker monsoon circulation in JJA(+1), with anomalous northeasterly winds near Somalia, and the beginning of slightly increased alongshore winds off Sumatra (Fig. 11f). During this time, slight westerlies are seen in the western and central equatorial Pacific Ocean. These transitions of surface temperature anomalies and wind circulation features show that there is a biennial component to the large-scale climate in this region.

Composites of precipitation anomalies from the model for the seasons starting with JJA(0) and going to SON(+1) are shown in Fig. 12. Strong positive anomalies of rainfall exist over the Indian subcontinent, Bay of Bengal, and the eastern equatorial Indian Ocean in JJA(0) (Fig. 12a), along with negative anomalies in the central Pacific Ocean coinciding with the cool T_s anomalies there. Negative anomalies develop in the western Indian Ocean north of the equator in SON(0) (Fig. 12b), and become stronger in DJF(+1) (Fig. 12c), with opposite sign anomalies of precipitation developing in the central and southeastern equatorial region. This pattern of precipitation is consistent with the patterns of surface

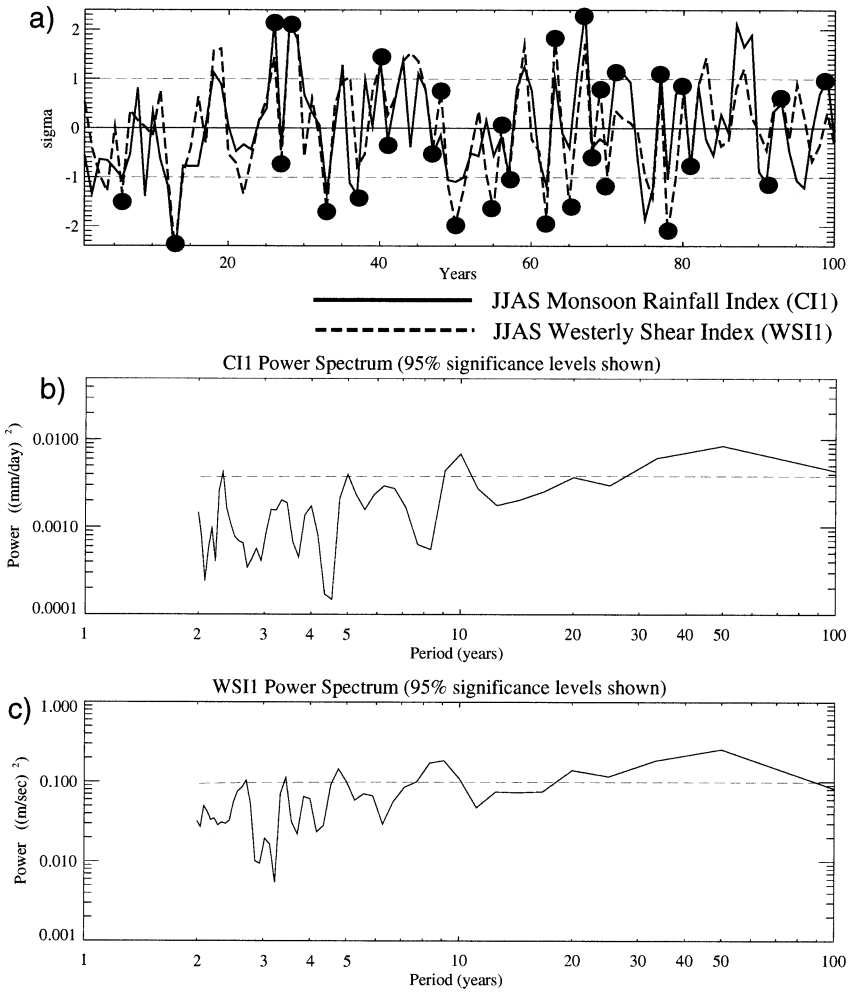

FIG. 10. (a) Time series of normalized CI1 and WSI1 anomalies. Black dots signify strong and weak TBO years, where both the CI1 and WSI1 are relatively greater or less than preceding and following years. (b) Power spectrum of the monthly values of CI1, with the 95% significance level shown as the dotted line. (c) Power spectrum of the monthly values of WSI1.

temperature and wind anomalies (i.e., an increased Walker-type circulation over the equatorial Indian Ocean, with increased surface westerlies). Note that when the composites are taken when the DMI is above or below one standard deviation (not shown), a pattern of precipitation emerges that closely resembles that of observations for strong IOZM years (Webster et al. 1999), with more precipitation anomalies over the continental regions of eastern Africa near the equator. The strong positive precipitation anomalies transition through into the regions over the Maritime Continent and northern Australia during SON(0) and DJF(+1), consistent with the SVD analysis in Figs. 5e,f. The following boreal summer monsoon over India in JJA(+1) (Fig. 12e) shows negative precipitation anomalies, and the Pacific Ocean displays slight positive precipitation anomalies in the equatorial region in the following season [SON(+1); Fig. 12f], both opposite in sign to anomalies the previous year, showing the biennial nature to the Indian–Pacific region.

Composites for oceanic temperature as a function of longitude and depth along the equator in the Indian Ocean are shown in Fig. 13. Also shown in Fig. 13 is the climatological depth of the 20°C isotherm for each season displayed. The basic features of the isotherm are very similar to that of observations (Xie et al. 2002). During the strong monsoon season of JJA(0) (Fig. 13b), warm subsurface temperature anomalies develop in the eastern equatorial areas near the coast of Sumatra, in association with the anomalously weak along- and offshore wind anomalies. The beginning of cool surface anomalies in the western equatorial region described in Fig. 11b can also be seen here. In the following season [SON(0); Fig. 13c], the warm subsurface anomalies in the east reach peak levels of near 1°C between 50 and 100 m of depth, while the cool western anomalies reach

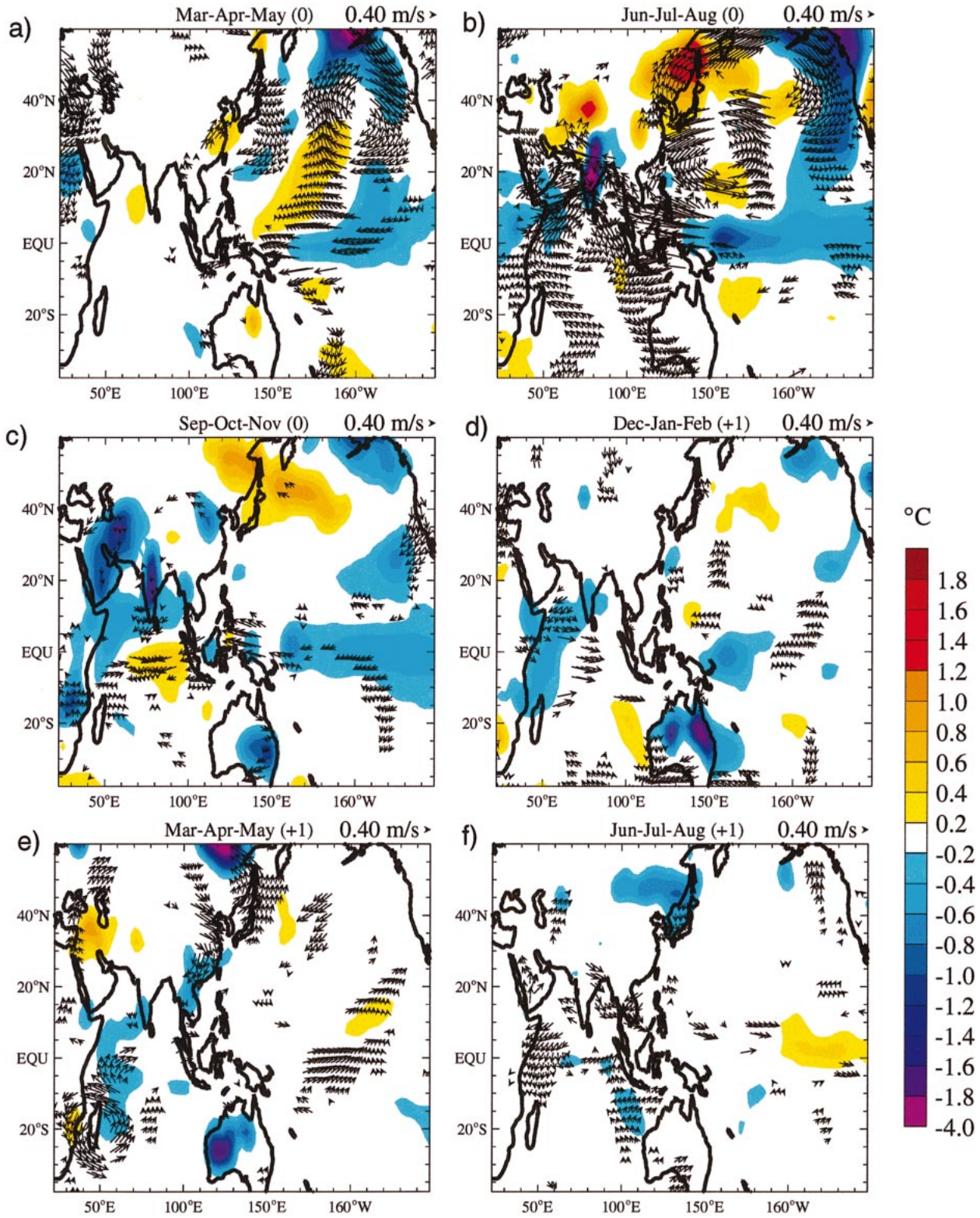

FIG. 11. Composite of anomalies of T_s and 850-mb winds for strong minus weak TBO years for (a) MAM(0); (b) JJA(0); (c) SON(0); (d) DJF(+1); (e) MAM(+1); and (f) JJA(+1). Only values above the 95% significance level are plotted.

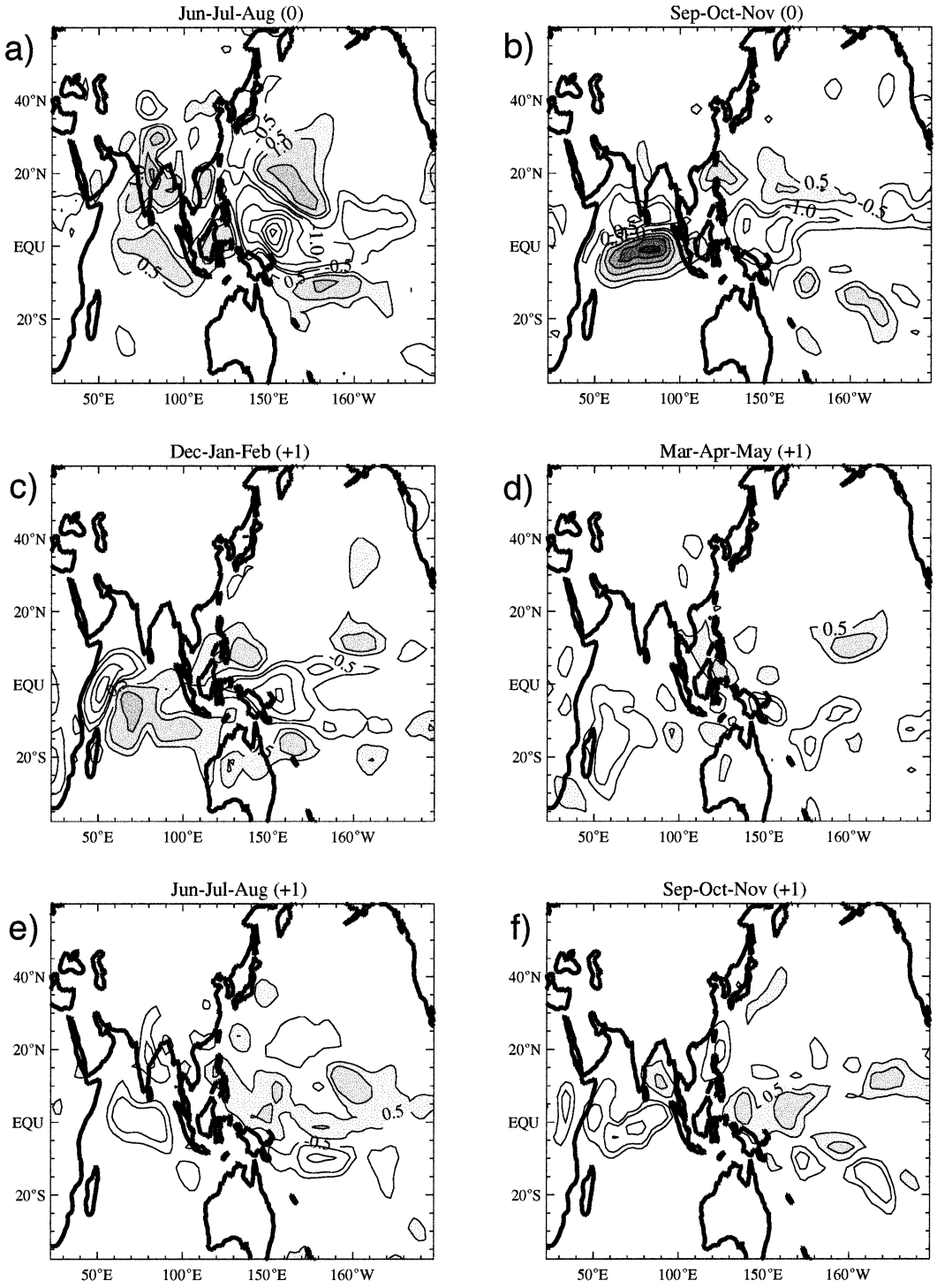

FIG. 12. Composite of anomalies of total precipitation for the strong minus weak TBO years for (a) JJA(0); (b) SON(0); (c) DJF(+1); (d) MAM(+1); (e) JJA(+1); and (f) SON(+1). Units are mm day^{-1}; contour levels are 0.5, 1.0, 2.0, 3.0, etc.; positive values above 0.5 mm day^{-1} are shaded.

levels near 0.5°C, similar to observational composites (MAL). In DJF(+1) (Fig. 13d), the anomalous subsurface temperature gradient persists, with slight reductions in the magnitudes of the warm eastern regions, but cool western anomalies persisting in magnitude and reaching depths of 100 m or more. In observations, the cool SST anomalies begin to cover the entire equatorial basin in DJF(+1) (MAL). One possible reason that the model

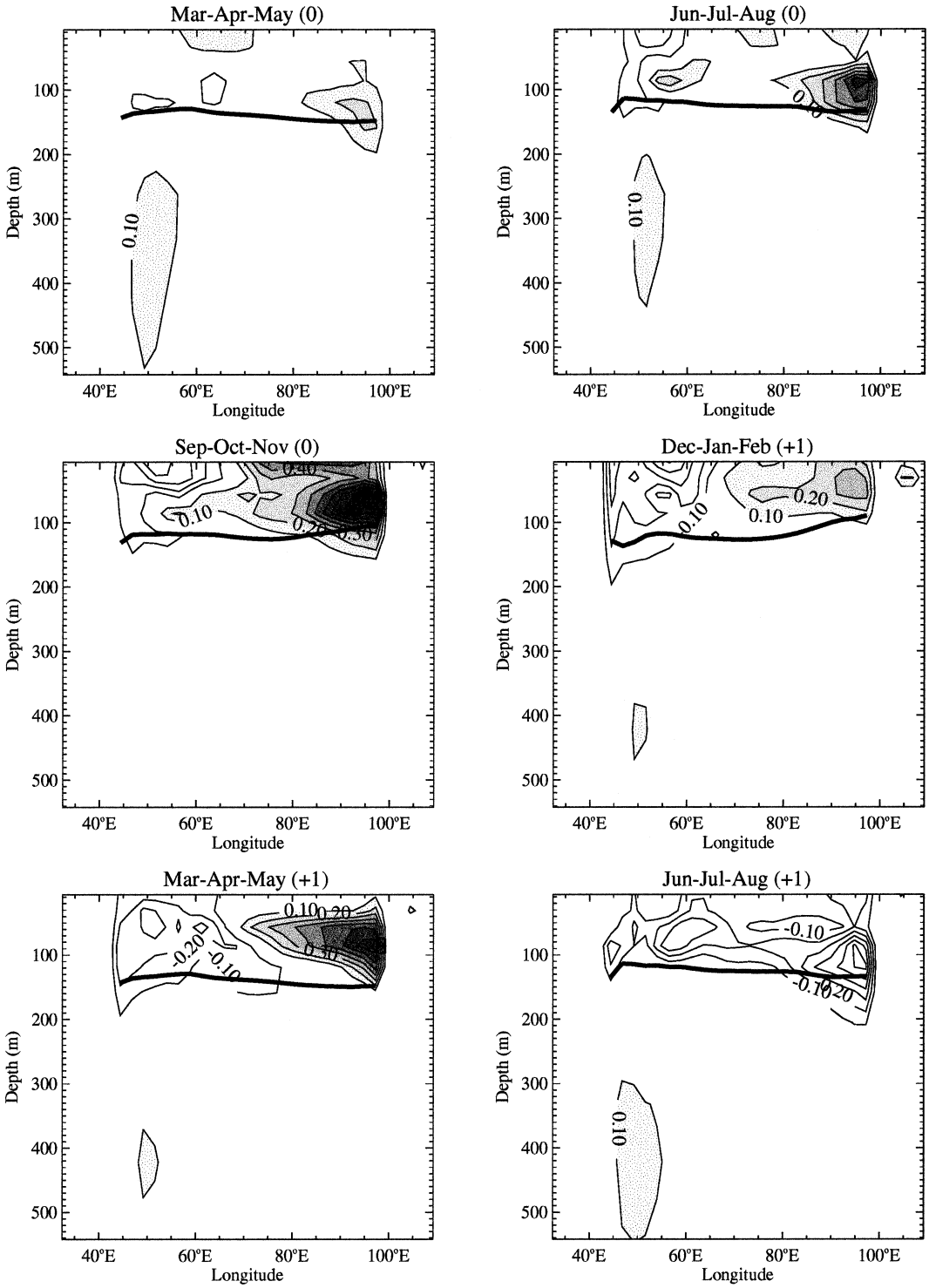

FIG. 13. Composite anomalies of oceanic temperature vs depth at 0.6°N in the Indian Ocean for strong minus weak TBO years for (a) MAM(0); (b) JJA(0); (c) SON(0); (d) DJF(+1); (e) MAM(+1); and (f) JJA(+1). Units are °C; contour level is 0.1°C; positive values above 0.1°C are shaded. Thick solid line in each plot is the climatological depth of the 20°C isotherm for that particular season.

fails to reproduce this feature is that this surface transition in the eastern Indian Ocean may be due to surface heat flux anomalies in DJF, related to wind and enhanced latent heat fluxes, causing the surface temperatures to become negative even though there are positive temperature anomalies just below the surface in the observations (MAL). This could be why the model does not ''shut off'' the dipole signature in the surface temperatures in the boreal winter season. In SON(0) (Fig. 13c), the temperature gradient at the subsurface may also be thought of as a large-scale tilting of the thermocline, with a shallow thermocline in the west and a deeper thermocline in the east. During the following boreal summer season [JJA(+1); Fig. 13f], large negative anomalies are seen at subsurface levels, displaying the biennial character of this process. The regions of strong subsurface temperature anomalies correspond to regions of anomalous upwelling and downwelling in the equatorial regions. When similar composites of oceanic vertical velocity at a depth of 50 m are made for strong minus weak years (not shown), strong anomalies of downwelling are seen in JJA(0) in the eastern equatorial Indian Ocean, and are associated with the wind anomalies discussed relative to Figs. 11b,c. These downwelling anomalies persist into the following season [SON(0)]. Anomalies of upwelling (and thus cooling) exist near the western equatorial region in JJA(0) and in the western off-equatorial regions in SON(0). Cold subsurface anomalies in the western equatorial section increase from Fig. 13d to Fig. 13e. In this region there is significant upwelling near the equator in the west in MAM(+1) that is related to the anomalous surface winds in MAM(+1) in Fig. 11e.

To analyze the influence of ocean dynamics on the development of surface and subsurface temperature anomalies that are a part of the IOZM and the TBO, we focus on the wave dynamics in the near-equatorial southern Indian Ocean, an area identified by Webster et al. (1999) as strongly influencing the IOZM. In that study, they showed a Hovmöller diagram of sea surface height anomalies during the strong positive IOZM event of 1997/98, and indicated the evidence of ocean Rossby waves driven by anomalies of near-equatorial zonal wind. We identify the possibility of ocean wave dynamics from signatures of ocean heat content in Fig. 14, which shows a Hovmöller diagram of composite model monthly heat content anomalies for the upper 125 m of the Indian Ocean for strong minus weak TBO years. The figure is calculated at a latitude of 9°S to examine the Rossby wave signal. The sign convention in Fig. 14 is opposite to that of Webster et al. (1999), as we are compositing a strong minus weak TBO year, and thus a negative minus positive IOZM year. Large regions of negative heat content are apparent in the eastern regions during the boreal spring and summer of the strong TBO year [e.g., May(0)]. These negative heat content anomalies then propagate westward and influence the western basin the following fall and winter seasons [e.g., Dec(0)]. During this period, opposite sign anomalies begin to propagate westward from the eastern basin and extend toward the central basin by the following fall season. This signal of oceanic Rossby waves in the southern Indian Ocean is similar to the observational results in Xie et al. (2002).

To illustrate the relationship of the Indian Ocean equatorial surface temperature gradient in the boreal fall season to the Indian summer monsoon, ENSO, and thus to the TBO, we compare the time series of the DMI (SON means) to the WSI1 and to the Niño-3.4 surface temperature anomaly. Figure 15a shows the WSI1 and the DMI for 100 yr of model output. Table 1 list the correlations of the DMI to WSI1 and to various other indices to be discussed below. The WSI1 and DMI have a fairly strong negative correlation (−0.66), showing that the cooling in the western equatorial region along with the warming in the east during the boreal fall season is related to the anomalously strong monsoon. In years when the monsoon is anomalously weak, the reverse is true, and the western regions are cool while the eastern regions are warm. The WSI1 also correlates strongly to the SON T_s anomaly in the eastern region off the coast of Sumatra (−0.59), illustrating how that region area is a key area in these processes (Annamalai et al. 2003, hereafter A03). Figure 15b shows the WSI and the index for the annual mean anomalous surface temperature in the Niño-3.4 region. [We use the annual mean Niño-3.4 T_s, similar to Meehl and Arblaster (1998), as the ENSO in the CSM is not as strongly phase-locked to the annual cycle as in observations.] The two indexes are negatively correlated (−0.83), showing a strong relationship between the Indian summer monsoon and the tropical Pacific in the CSM. Strong summer monsoon years are associated with negative T_s anomalies (La Niña in extreme years) in the Pacific, and vice versa for weak monsoon years. Note that the incidences of protracted multiyear El Niño or La Niña events also coincide with multiyear anomalies of the same sign of the WSI1 (e.g., years 42–44, 49–51). Contrary to other modeling studies (Iizuka et al. 2000), the results from the CSM also suggest that the IOZM is also strongly linked to the tropical Pacific. Figure 15c shows the Niño-3.4 index along with the DMI, which correlate at +0.56. The relatively strong correlations of all three indices to each other illustrates that the DMI is a part of the large-scale Indian–Pacific Ocean climate and is an inherent feature of the TBO–ENSO–monsoon system. This result is similar to observations (A03). In the 100 yr of model output analyzed in this study, there are 15 strong and 15 weak WSI1 years (as measured by ±1 standard deviation). Of the strong WSI1 years, 10 are negative IOZM years, and none are positive IOZM years (as measured by ±1 standard deviation of the DMI). When the WSI1 is weak, eight of those years are positive IOZM years, and one is negative. Similar relationships apply to the ENSO–IOZM comparison, as 7 of the 16 El Niño years (as

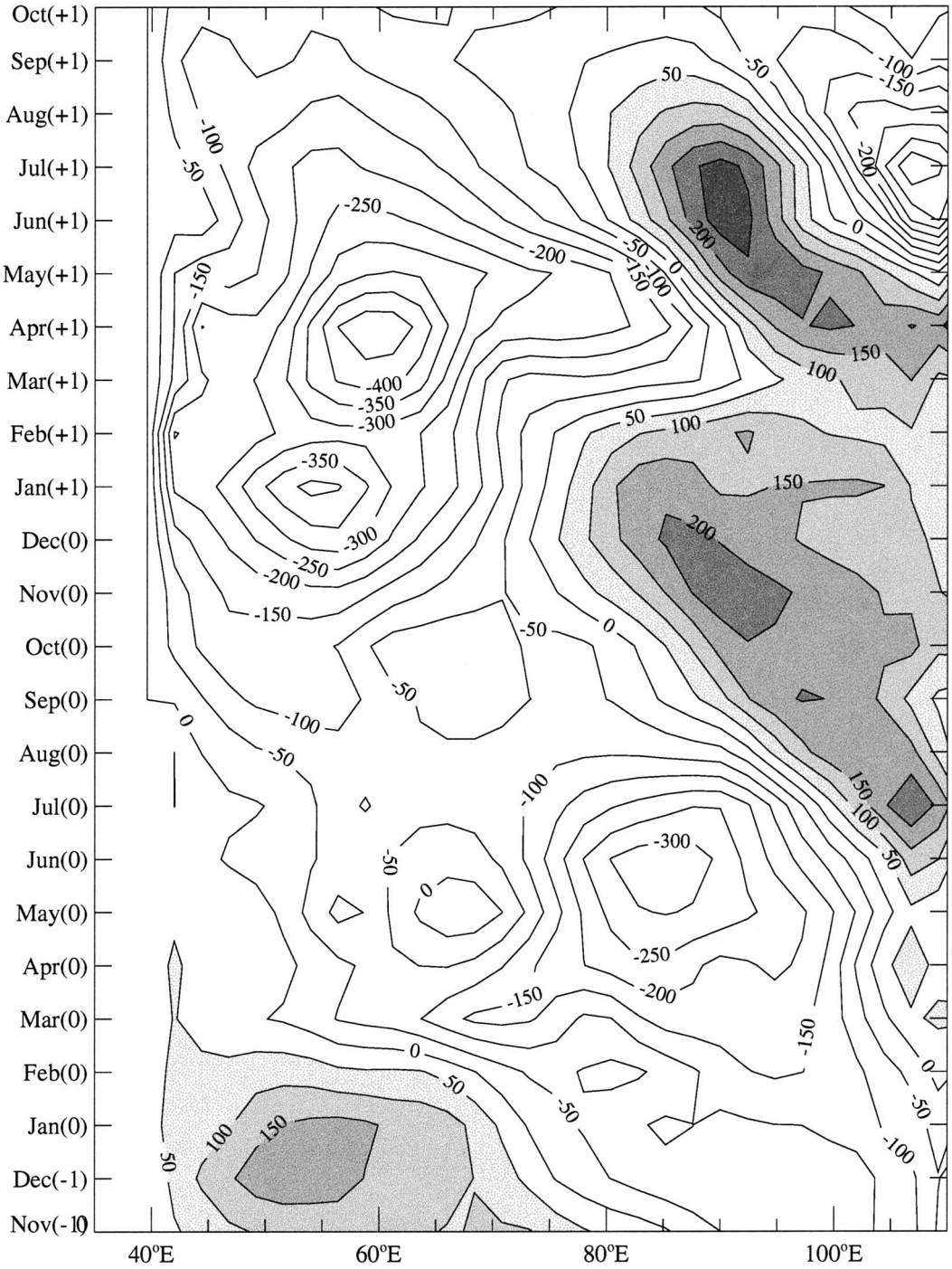

FIG. 14. Hovmöller diagram of composite model monthly heat content differences (°C m) calculated over the top 125 m of the Indian Ocean for strong minus weak TBO years. Time increases upward starting with the boreal winter before the relatively strong Indian monsoon [e.g., Jan(0)], and continuing through the following boreal summer with a relatively weak Indian monsoon [e.g., Jul(+1)]. Contour level is 50°C m. Regions of positive values above 50°C m are shaded.

measured by ±1 standard deviation of the Niño-3.4 index) are positive IOZM years, and none are negative IOZM years. Of the 17 La Niña years, 8 are negative IOZM years, and only 1 is positive. Of the 12 positive IOZM years, 7 are El Niño years. Although not all IOZM events occur in ENSO (or strong/weak monsoon) years, the close connection of the IOZM to ENSO (and to TBO and the monsoon) is in strong contrast to other

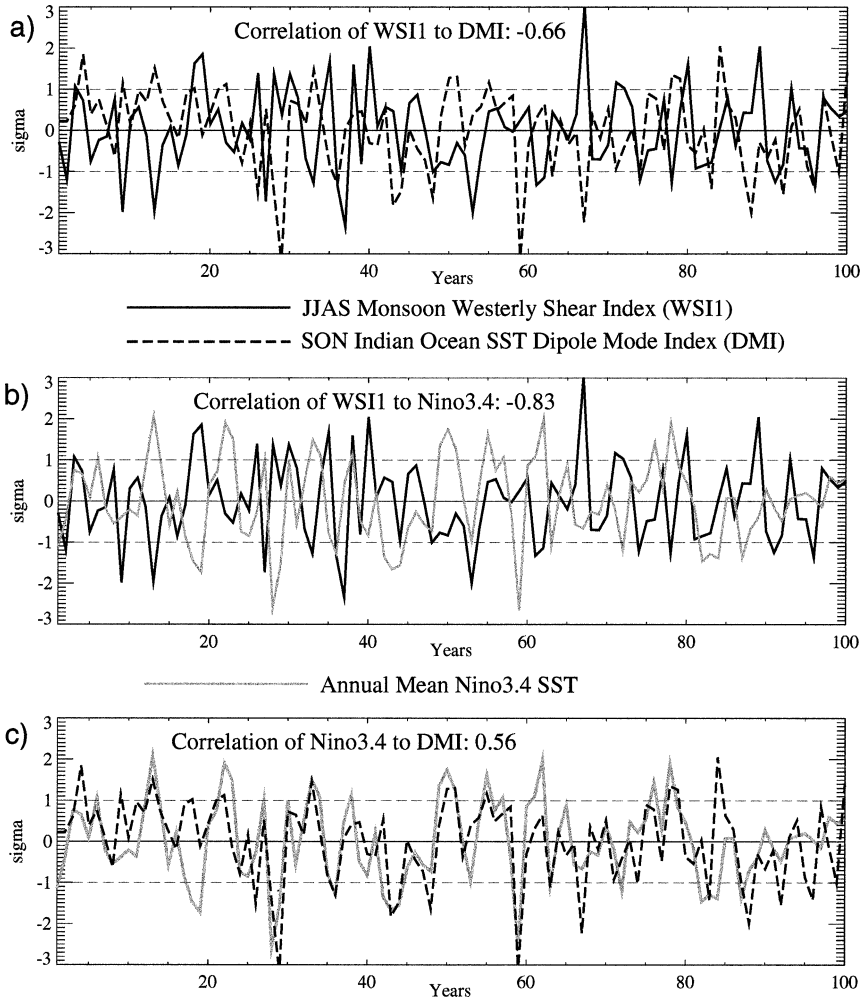

FIG. 15. (a) Time series of the indexes related to JJAS monsoon strength (WSI1, solid line) and the SON DMI (SST anomalies from 5°S–10°N, 40°–55°E minus 10°S–5°N, 90°–102°E, dashed line). (b) Time series of the WSI1 (solid line) and the annual mean eastern equatorial Pacific T_s anomalies (Niño-3.4, gray line). (c) Time series of the Niño-3.4 T_s anomaly index (gray line) and the SON DMI (dashed line). Correlations of various pairs are shown.

recent research (Iizuka et al. 2000). It will be the aim of a future study to determine the causes of the ''exceptional'' IOZM cases.

e. Cross-equatorial oceanic meridional heat transport

Loschnigg and Webster (2000) examined the interannual variability of the meridional cross-equatorial oceanic heat transport of the Indian Ocean. In their study, it was hypothesized that the heat transport may be part of a coupled ocean–atmosphere system of SST modulation that may affect the interannual variability of the Indian summer monsoon by decreasing (increasing) the mean heat content in the northern Indian Ocean regions during strong (weak) monsoons. This anomalous heat content would affect the SST in the following seasons and thus influence the strength of the subsequent summer monsoon through Indian Ocean SST–monsoon relationships (Clark et al. 2000).

The CSM accurately simulates both the annual mean and seasonal cycle of the cross-equatorial heat transports in the Indian Ocean. The climatological annual mean

TABLE 1. Correlations of model indexes: WSI1 (JJAS $U_{850} - U_{200}$ wind shear anomalies, 5°–15°N, 35°–75°E), DMI (SON T_s anomaly difference between 5°S–10°N, 40°–55°E and 10°S–5°N, 90°–102°E), Niño-3.4 (annual mean T_s anomaly, 5°S–5°N, 170°–120°W), Sumatra (SON T_s anomaly, 10°S–5°N, 90°–102°E), Q_v (JJAS oceanic meridional heat transport across the equator in the Indian Ocean). All values are significant at the 99.9% level.

Index	DMI	Sumatra	Niño-3.4	Q_v
WSI1	−0.66	−0.59	−0.83	−0.56
Niño-3.4	+0.56	−0.52	—	0.38
Q_v	−0.41	−0.40	0.38	—

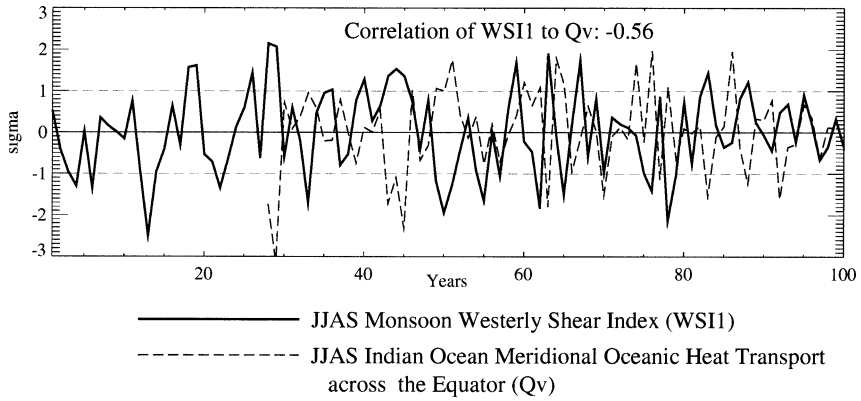

FIG. 16. Time series of the WSI1 (solid line) and the oceanic cross-equatorial meridional heat transport during JJAS (Q_v, dashed line). Negative values of Q_v denote anomalously strong southward heat transport. The correlation of the two indices is shown.

cross-equatorial heat transport is −0.3 PW (1 PW = 10^{15} W, with the negative sign denoting southward heat transport), and the JJAS climatological mean is −1.0 PW, well within the ranges of other observational and modeling studies [see Schott and McCreary (2001) for a review of heat transport estimates for the Indian Ocean]. The heat transport calculations were integrated through all ocean levels to the depth of the Indian Ocean basin. Figure 16 shows a time series of the heat transport (Q_v) across the equator in the Indian Ocean in the CSM during the peak boreal summer monsoon months (JJAS) correlated with the WSI1 index. (Results for the heat transport are displayed only from year 27 onward, due to model output availability described in section 2.) The two timeseries have a fairly strong negative correlation (−0.56; see Table 1), showing that in years of strong monsoon circulation, there is anomalously strong southward (negative) heat transport in the Indian Ocean. This anomalous heat transport affects heat content in the northern Indian Ocean and contributes to patterns of anomalous SST that can persist through multiple seasons to enhance the TBO transition of the monsoon the following boreal spring season.

The basic process is that in the strong monsoon cycle, there would be more southward oceanic heat transport in JJAS from the increased Ekman transports. This increased transport would be a contributing factor in leaving negative heat content anomalies in the north Indian Ocean (Loschnigg and Webster 2000), along with the other processes identified in observations by Meehl and Arblaster (2002b) that influence the development of SST anomalies in this region. The transition of heat content anomalies is illustrated in Figs. 13a–d, which show that the upper ocean temperature anomalies start out mostly warm and begin to transition to cold in the western Indian Ocean in JJAS (coincident with the anomalous southward heat transports) and end up with the entire Indian Ocean cold to influence the monsoon the following JJA+1, consistent with the T_s anomaly evolution in Fig. 11. This transition of cool heat content anomalies appearing first in the western Indian Ocean is also consistent with the results of Loschnigg and Webster (2000), who showed the peak heat transports influencing the Arabian Sea region in the north Indian Ocean. The timescale is such that the SST anomalies developed through the contribution of the heat transport, along with other processes, persist in this region through several seasons and help develop a weak monsoon cycle the next year, as SST anomalies in the north Indian Ocean have been shown to lead to monsoon variability (Clark et al. 2000; Meehl and Arblaster 2001, 2002b). Thus the cross-equatorial oceanic heat transport is another mechanism whereby coupled dynamics in the Indian Ocean contribute to the TBO that also encompasses the ENSO–monsoon system.

4. Discussion and conclusions

The NCAR CSM is shown to adequately simulate the seasonal cycle of temperature, precipitation, and winds associated with the Asian–Australian monsoon. SVD analyses show the model captures the salient features of the TBO boreal spring transition conditions, as well as the subsequent boreal fall patterns that influence Australian monsoon rainfall. Single and cumulative anomaly pattern correlations are also comparable to observations in that the contribution of the transition conditions vary more from year to year in the Indian monsoon compared to the Australian monsoon. This indicates that, for the model as in observations, contributions of varying strength from year to year can ultimately end up influencing the Indian monsoon. But as those conditions set the strength of the Indian monsoon, there is a consistency of the coupled interaction in the system that carries over to the Australian monsoon. That is, once set, a strong Indian monsoon often leads to a strong Australian monsoon, and vice versa for a weak Indian monsoon.

The coupled ocean dynamics that contribute to the IOZM are shown to be an integral part of the TBO–

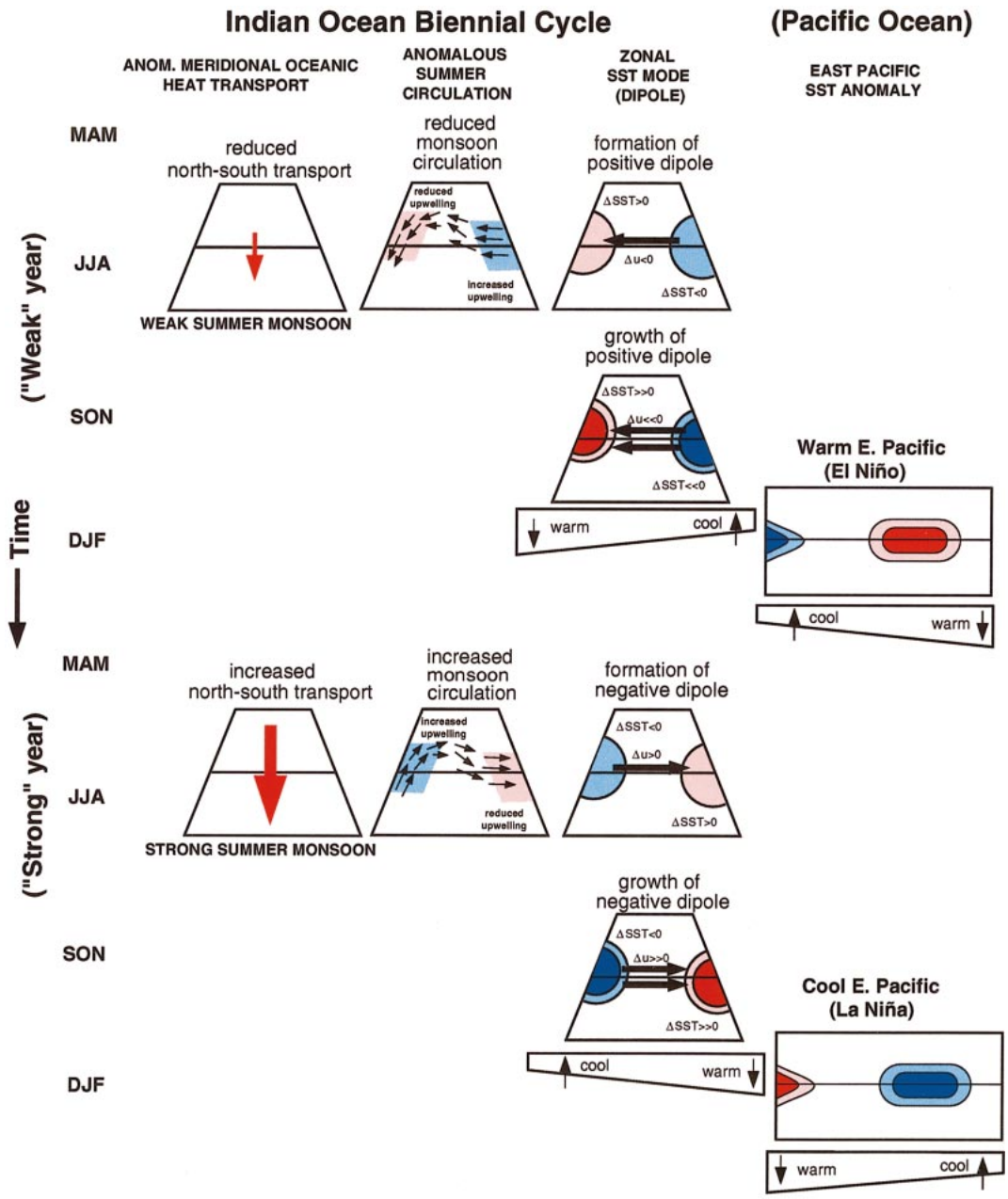

FIG. 17. Schematic of the biennial cycle of the Indian and Pacific Oceans, including the IOZM, or dipole mode. The black arrows show the anomalous surface winds, and the red arrow shows the relative strength of the southward oceanic heat transports in the Indian Ocean. Colored regions represent the anomalous warm (red) and cool (blue) SST. Anomalous thermocline tilting is shown underneath the schematic of each basin, with the arrows denoting anomalous upwelling and downwelling. Adapted from W03.

monsoon system in the Indian Ocean. Through anomalies in upwelling at both the eastern and western sides of the equatorial Indian Ocean, the strength of the monsoon wind circulation affects the ocean dynamics and enhances SST anomalies in this region. The strength of the monsoon winds also affects the magnitudes of the southward summertime oceanic heat transport, which contribute to developing ocean heat content and SST anomalies. To a large degree, the interrelationship of the components of the Indian Ocean and the monsoon, as suggested by W03 are corroborated by associations found in the NCAR CSM. The interaction of these processes are displayed in Fig. 17 (adapted from W03), which shows a schematic of a biennial cycle for the Indian Ocean involving the ocean dynamics in the equatorial region. As the starting period is arbitrary, we begin

in the boreal summer season during a ''weak'' monsoon (JJA). The reduced monsoon surface wind circulation causes reduced upwelling in the western equatorial regions, and enhanced upwelling in the eastern equatorial regions near Sumatra, due to the strong along- and offshore winds there. This begins the development of SST anomalies that are characteristic of a ''positive'' dipole. Also during this period, the weaker monsoon circulation produces lower-than-average southward heat transport, leaving larger heat content anomalies in the northern oceanic areas in the following seasons. Loschnigg and Webster (2000) showed that this coupled interaction of the monsoon circulation and the heat transport could be a contributing factor in assisting the development of heat content anomalies and thus SST anomalies that can affect the interannual variability of the monsoon. They showed that these heat content anomalies can persist until the following boreal spring season, and that the resulting SST anomalies affect the development of the subsequent Indian monsoon. The heat transports can be considered one of the many factors that contribute to the transition of the TBO cycle. In the boreal fall months (SON of the weak year), the SST dipole reaches its maximum magnitude with the anomalous equatorial surface easterlies enhancing the SST anomalies on either side of the basin, and tilting the thermocline along the equator, raising it in the east and depressing it in the west. This situation is similar to the sign of anomalies during the 1997/98 period in the Indian Ocean. During this time (SON to DJF), the Pacific develops warm SST anomalies in the central and eastern part of the basin, with El Niño conditions prevailing, and an opposite tilt of the equatorial thermocline to that of the Indian Ocean. The SST anomalies that develop through the dipole and that are enhanced through the anomalous heat transport persist through the winter season and contribute to the development of a ''strong'' monsoon the following boreal summer (JJA). Stronger-than-normal monsoon surface wind circulation causes upwelling and downwelling anomalies at either sides of the equator in the Indian Ocean that are reversed as compared to those of the previous year. Also, the increased monsoon winds drive an increased southward heat transport, reducing heat content in the northern Indian Ocean. The heat content anomalies developed during this strong monsoon season persist until the following spring season, affecting the TBO transition and the subsequent monsoon as mentioned earlier. These processes in the boreal summer period (JJA of the strong year) begin to develop a ''negative'' dipole in the summer months, which then reaches peak magnitude in the boreal fall with the influence of the equatorial westerlies (SON). These westerlies also help tilt the thermocline in an opposite direction to the previous summer, with a raised thermocline in the west and a depressed one in the east. In the Pacific, La Niña conditions are present, with cool SST anomalies in the central equatorial basin and an opposite tilt to the thermocline to that of the Indian Ocean (DJF).

The results here show that, contrary to a previous modeling study (Iizuka et al. 2000), the IOZM is not independent of the tropical Pacific and ENSO. Rather, it is an integral part of the TBO and thus the ENSO–monsoon system. Also, consistent with several studies (Baquero-Bernal et al. 2002; Nicholls 2001; Allan et al. 2001), the only season with a significant SST gradient in the equatorial Indian Ocean region is the boreal fall (SON). The IOZM is thus an inherent feature of the interannual variability of the large-scale Indian–Pacific Ocean region climate, and is not an independently oscillating mode of the Indian Ocean. As noted previously, despite the strong connection of the TBO and ENSO to the DMI, there are a small number of dipole events that occur in years without an El Niño or La Niña. These ''exceptional'' cases will be dealt with in a future paper.

Another feature of the TBO that may have a significant effect on the near-equatorial SST anomalies is the existence of equatorial and off-equatorial oceanic waves that may enhance the Indian Ocean zonal SST gradient. In the strong positive SST dipole event of 1997/98, it was hypothesized that equatorial waves contributed to a positive feedback, which enhanced the SST anomalies, particularly on the western side of the Indian Ocean Basin (Webster et al. 1999). The basic idea is that the easterlies in the boreal fall would produce an upwelling Kelvin wave that would raise the thermocline in the east, maintaining the cooling off Sumatra. The equatorial easterlies would also develop an off-equatorial Rossby wave that would propagate westward and deepen the thermocline in the western Indian Ocean. This Rossby wave was very evident in TOPEX data during 1997/98, with most of the strength near 5° to 10°S (Webster et al. 1999), similar to the model results shown in Fig. 14 (but with opposite sign anomalies). It is also possible that Kelvin waves reflected from the eastern coast would produce Rossby waves that propagate westward and enhance the thermocline depth there. Meehl and Arblaster (2002b) consider the equatorial waves to be a part of the transitions of SST anomalies in the Indian Ocean (as well as the Pacific), and thus a part of the biennial cycle for this region. We intend to analyze this equatorial wave activity in the NCAR CSM in relation to the TBO and the IOZM more fully in a future paper.

Acknowledgments. This work has been supported by NASA Grant NAG 5-7485, and National Science Foundation, Division of Atmospheric Sciences Grant ATM-9525847 and ATM-0120956. The authors thank the anonymous reviewers for helpful comments on the manuscript. The International Pacific Research Center is partly sponsored by Frontier Research System for Global Change.

REFERENCES

Allan, R., and R. D. D'Arrigo, 1999: 'Persistent' ENSO sequences: How unusual was the 1990–95 El Niño? *Holocene*, **9,** 101–118.

——, and Coauthors, 2001: Is there an equatorial Indian Ocean SST Dipole, and is it independent of the El Niño Southern Oscillation. *CLIVAR Exch.,* **6,** 18–22.

Annamalai, H., R. Murtugudde, J. Potemra, S. Xie, and B. Wang, 2003: Coupled dynamics in the Indian Ocean: Spring initiation of the zonal mode. *Deep-Sea Res.,* in press.

Arblaster, J. M., G. A. Meehl, and A. Moore, 2002: Interdecadal modulation of Australian rainfall. *Climate Dyn.,* **18,** 519–531.

Baquero-Bernal, A., M. Latif, and S. Legutke, 2002: On dipolelike variability of SST in the tropical Indian Ocean. *J. Climate,* **15,** 1358–1368.

Behera, S. K., P. S. Salvekar, and T. Yamagata, 2000: Simulation of interannual SST variability in the tropical Indian Ocean. *J. Climate,* **13,** 3487–3499.

Bonan, G. B., 1998: The land surface climatology of the NCAR Land Surface Model coupled to the NCAR Community Climate Model. *J. Climate,* **11,** 1307–1326.

Boville, B., and P. Gent, 1998: The NCAR Climate System Model, version one. *J. Climate,* **11,** 1115–1130.

Chang, C. P., and T. Li, 2000: A theory for the tropical tropospheric biennial oscillation. *J. Atmos. Sci.,* **57,** 2209–2224.

Clark, C. O., J. E. Cole, and P. J. Webster, 2000: Indian Ocean SST and Indian summer rainfall: Predictive relationships and their decadal variability. *J. Climate,* **13,** 2503–2519.

Clarke, A., X. Liu, and S. Van Gorder, 1998: Dynamics of the biennial oscillation in the equatorial Indian and far western Pacific Oceans. *J. Climate,* **11,** 987–1001.

Garternicht, U., and F. Schott, 1997: Heat fluxes of the Indian Ocean from a global eddy-resolving model. *J. Geophys. Res.,* **102,** 21 147–21 159.

Gent, P. R., F. O. Bryan, G. Danabasoglu, S. C. Doney, W. R. Holland, W. G. Large, and J. C. McWilliams, 1998: The NCAR Climate System Model global ocean component. *J. Climate,* **11,** 1287–1306.

Goswami, B. N., 1995: A multiscale interaction model for the origin of the tropospheric QBO. *J. Climate,* **8,** 524–534.

Hastenrath, S., and L. Greischar, 1993: The monsoonal heat budget of the hydrosphere-atmosphere system in the Indian Ocean sector. *J. Geophys. Res.,* **98,** 6869–6881.

Hsiung, J., R. E. Newell, and T. Houghtby, 1989: The annual cycle of oceanic heat storage and oceanic meridional heat transport. *Quart. J. Roy. Meteor. Soc.,* **115,** 1–28.

Iizuka, S., T. Matsuura, and T. Yamagata, 2000: The Indian Ocean SST dipole simulated in a coupled general circulation model. *Geophys. Res. Lett.,* **27,** 3369–3372.

Kalnay, E., and Coauthors, 1996: The NCEP/NCAR 40-Year Reanalysis Project. *Bull. Amer. Meteor. Soc.,* **77,** 437–471.

Kawamura, R., T. Matsuura, and S. Iizuka, 2001: Role of an equatorially asymmetric mode in the Indian Ocean in the Asian summer monsoon-ENSO coupling. *J. Geophys. Res.,* **106,** 4681–4693.

Kiehl, J. T., J. J. Hack, G. B. Bonan, B. A. Boville, D. L. Williamson, and P. J. Rasch, 1998: The National Center for Atmospheric Research Community Climate Model: CCM3. *J. Climate,* **11,** 1131–1150.

Kim, K. M., and K. M. Lau, 2001: Dynamics of monsoon-induced biennial variability in ENSO. *Geophy. Res. Lett.,* **28,** 315–318.

Kitoh, A., S. Yukimoto, and A. Noda, 1999: ENSO-monsoon relationship in the MRI coupled GCM. *J. Meteor. Soc. Japan,* **77,** 1221–1245.

Lau, K.-M., and H.-T. Wu, 1999: Assessment of the impacts of the 1997–98 El Niño on the Asian–Australian monsoon. *Geophys. Res. Lett.,* **26,** 1747–1750.

Lee, T., and J. Marotzke, 1997: Inferring meridional mass and heat transports of the Indian Ocean by fitting a general circulation model to climatological data. *J. Geophys. Res.,* **102,** 10 585–10 602.

Li, T., C. W. Tham, and C. P. Chang, 2001: A coupled air–sea–monsoon oscillator for the tropospheric biennial oscillation. *J. Climate,* **14,** 752–764.

Loschnigg, J., and P. J. Webster, 2000: A coupled ocean–atmosphere system of SST modulation in the Indian Ocean. *J. Climate,* **13,** 3342–3360.

Meehl, G. A., 1987: The annual cycle and interannual variability in the tropical Pacific and Indian Ocean regions. *Mon. Wea. Rev.,* **115,** 27–50.

——, 1993: A coupled air–sea biennial mechanism in the tropical Indian and Pacific Ocean regions: Role of the ocean. *J. Climate,* **6,** 31–41.

——, 1994: Coupled land–ocean–atmosphere processes and South Asian monsoon variability. *Science,* **266,** 263–267.

——, 1997: The south Asian monsoon and the tropospheric biennial oscillation. *J. Climate,* **10,** 1921–1943.

——, and J. M. Arblaster, 1998: The Asian–Australian Monsoon and El Niño–Southern Oscillation in the NCAR Climate System Model. *J. Climate,* **11,** 1356–1385.

——, and ——, 2001: The tropospheric biennial oscillation and Indian monsoon rainfall. *Geophys. Res. Lett.,* **28,** 1731–1734.

——, and ——, 2002a: Indian monsoon GCM sensitivity experiments testing tropospheric biennial oscillation transition conditions. *J. Climate,* **15,** 923–944.

——, and ——, 2002b: The tropospheric biennial oscillation and Asian–Australian monsoon rainfall. *J. Climate,* **15,** 722–744.

——, ——, and J. Loschnigg, 2003: Coupled ocean–atmosphere dynamical processes in the tropical Indian and Pacific Oceans and the TBO. *J. Climate,* in press.

Murtugudde, R., J. P. McCreary, and A. J. Busalacci, 2000: Oceanic processes associated with anomalous events in the Indian Ocean with relevance to 1997–98. *J. Geophys. Res.,* **105,** 3295–3306.

Nicholls, N., 2001: Is there an equatorial Indian Ocean SST Dipole, independent of the El Niño Southern Oscillation. Preprints, *Symp. on Climate Variability, the Oceans, and Societal Impacts,* Albuquerque, NM, Amer. Meteor. Soc., 17–18.

Ogasawara, N., A. Kitoh, T. Yasunari, and A. Noda, 1999: Tropospheric biennial oscillation of ENSO-monsoon system in the MRI coupled GCM. *J. Meteor. Soc. Japan,* **77,** 1247–1270.

Parthasarathy, B., K. Rupa Kumar, and A. A. Munot, 1991: Evidence of secular variations in Indian monsoon rainfall–circulation relationships. *J. Climate,* **4,** 927–938.

Reason, C. J. C., R. J. Allan, J. A. Lindesay, and T. J. Ansell, 2000: ENSO and climatic signals across the Indian Ocean Basin in the global context: Part 1. Interannual composite patterns. *Int. J. Climatol.,* **20,** 1285–1387.

Ropelewski, C. F., M. S. Halpert, and X. Wang, 1992: Observed tropospheric biennial variability and its relationship to the Southern Oscillation. *J. Climate,* **5,** 594–614.

Saji, N. H., B. N. Goswami, P. N. Vinayachandran, and T. Yamagata, 1999: A dipole mode in the tropical Indian Ocean. *Nature,* **401,** 360–363.

Schott, F. A., and J. P. McCreary, 2001: The monsoon circulation of the Indian Ocean. *Progress in Oceanography,* Vol. 51, Pergamon, 1–123.

Tomita, T., and T. Yasunari, 1996: Role of the northeast winter monsoon on the biennial oscillation of the ENSO/monsoon system. *J. Meteor. Soc. Japan,* **74,** 399–413.

Torrence, C., and P. J. Webster, 1998: The annual cycle of persistence in the El Niño–Southern Oscillation. *Quart. J. Roy. Meteor. Soc.,* **124,** 1985–2004.

Trenberth, K. E., and T. J. Hoar, 1996: The 1990–1995 El Niño-Southern Oscillation event: Longest on record. *Geophys. Res. Lett.,* **23,** 57–60.

Venzke, S., M. Latif, and A. Villwock, 2000: The Coupled GCM ECHO-2. Part II: Indian Ocean Response to ENSO. *J. Climate,* **13,** 1371–1383.

Wacongne, S., and R. C. Pacanowski, 1996: Seasonal heat transport in the tropical Indian Ocean. *J. Phys. Oceanogr.,* **26,** 2666–2699.

Wang, B., and Z. Fan, 1999: Choice of south Asian summer monsoon indices. *Bull. Amer. Meteor. Soc.,* **80,** 629–638.

Weatherly, J. W., B. P. Briegleb, W. G. Large, and J. A. Maslanik, 1998: Sea ice and polar climate in the NCAR CSM. *J. Climate,* **11,** 1472–1486.

Webster, P. J., and S. Yang, 1992: Monsoon and ENSO: Selectively interactive systems. *Quart. J. Roy. Meteor. Soc.,* **118,** 877–926.
——, V. Magana, T. N. Palmer, J. Shukla, R. Tomas, T. M. Yanai, and T. Yasunari, 1998: The monsoon: Processes, predictability and the prospects for prediction. *J. Geophys. Res.,* **103,** 14 451–14 510.
——, A. Moore, J. P. Loschnigg, and R. Leben, 1999: Coupled ocean-atmosphere dynamics in the Indian Ocean during 1997–1998. *Nature,* **401,** 356–360.
——, J. Loschnigg, G. Cherikova, J. Fasullo, and W. Han, cited 2003: The coupled nature of the monsoon. [Manuscript available online at http://paos.colorado.edu/webster/selfreg/index.html.]
Xie, P., and P. A. Arkin, 1996: Analysis of global monthly precipitation using gauge observations, satellite estimates, and numerical model predictions. *J. Climate,* **9,** 840–858.
Xie, S. P., H. Annamalai, F. A. Schott, and J. P. McCreary, 2002: Structure and mechanism of South Indian Ocean climate variability. *J. Climate,* **15,** 864–878.
Yang, S., K. M. Lau, and M. Sankar-Rao, 1996: Precursory signals associated with the interannual variability of the Asian Monsoon. *J. Climate,* **9,** 949–964.
Yasunari, T., 1990: Impact of Indian monsoon on the coupled atmosphere/ocean system in the tropical Pacific. *Meteor. Atmos. Phys.,* **44,** 29–41.
——, 1991: The monsoon year—A new concept of the climatic year in the Tropics. *Bull. Amer. Meteor. Soc.,* **72,** 1331–1338.
——, and Y. Seki, 1992: Role of the Asian monsoon on the interannual variability of the global climate system. *J. Meteor. Soc. Japan,* **70,** 177–189.
Zebiak, S. E., and M. A. Cane, 1987: A model El Niño–Southern Oscillation. *Mon. Wea. Rev.,* **115,** 2262–2278.